



## West Africa in Rodinia: High quality paleomagnetic pole from the ~860 Ma Manso dyke swarm (Ghana)



Paul Yves Jean Antonio <sup>a,b,\*</sup>, Lenka Baratoux <sup>b</sup>, Ricardo Ivan Ferreira Trindade <sup>a</sup>, Sonia Rousse <sup>b</sup>, Anani Ayite <sup>c</sup>, Cristiano Lana <sup>d</sup>, Mélina Macouin <sup>b</sup>, Emmanuel Williams Kobby Adu <sup>e</sup>, Caroline Sanchez <sup>f</sup>, Marco Antônio Leandro Silva <sup>d</sup>, Anne-Sophie Firmin <sup>b</sup>, Carmen Irène Martínez Dopico <sup>g</sup>, Arnaud Proietti <sup>h</sup>, Prince Ofori Amponsah <sup>e</sup>, Patrick Asamoah Sakyi <sup>e</sup>

<sup>a</sup> Universidade de São Paulo (USP), Instituto de Astronomia, Geofísica e Ciências Atmosféricas (IAG), Rua do Matão, 1226, Cidade Universitária, 05508-090 São Paulo, SP, Brazil

<sup>b</sup> Université Paul Sabatier (UPS) - Toulouse III, Observatoire Midi-Pyrénées (OMP), Géosciences Environnement Toulouse (GET), 14 Avenue Edouard Belin, 31400 Toulouse, France

<sup>c</sup> Ghana Geological Survey Authority, 6, 7th Avenue West Ridge, Box M80, Accra, Ghana

<sup>d</sup> Universidade Federal de Ouro Preto (UFOP), Applied Isotope Research Group, Departamento de Geologia, Escola de Minas, Rua Diogo de Vasconcelos, 122, 35400-000 Ouro Preto, MG, Brazil

<sup>e</sup> Department of Earth Science, School of Physical and Mathematical Sciences, University of Ghana, P.O. Box LG 58, Legon-Accra, Ghana

<sup>f</sup> GEOPS, Université Paris-Sud, CNRS, Université Paris-Saclay, Rue du Belvédère, Bât. 504, 91405 Orsay, France

<sup>g</sup> INGEIS- Instituto de Geocronología y Geología Isotópica, Av. Int. Güiraldes, Ciudad Universitaria, Ciudad Autónoma de Buenos Aires, Argentina

<sup>h</sup> Centre de Microcaractérisation Raimond Castaing, 3 Rue Caroline Aigle, 31400 Toulouse, France

### ARTICLE INFO

#### Article history:

Received 23 November 2020

Received in revised form 22 January 2021

Accepted 25 February 2021

Available online 5 March 2021

Handling Editor: J.G. Meert

#### Keywords:

West Africa

Neoproterozoic

Tonian

Rodinia

Paleomagnetism

### ABSTRACT

The paleogeography of the Meso-Neoproterozoic Rodinia supercontinent remains debated partly because many stable cratons still lack reliable paleomagnetic data for this period. A new geochronological and paleomagnetic study was conducted on the NNW-trending Manso dyke swarm of southern West Africa (Ghana) to clarify the position of this unconstrained continent in Rodinia. Two U–Pb apatite ages of  $857.2 \pm 8.5$  Ma and  $855 \pm 16$  Ma agree with one previous baddeleyite age, indicating a ~860 Ma emplacement age for the Manso dykes. A characteristic remanent magnetization (ChRM) was isolated in stable single to pseudo-single domain (SD-PSD) magnetite. Well constrained site mean directions obtained for 13 dykes lead to a mean direction for the Manso dyke swarm of  $D_m = 181.9^\circ$ ,  $I_m = -77.2^\circ$  ( $N = 13$ ,  $\alpha_{95} = 7.6^\circ$ ,  $k = 30.6$ ), yielding a paleomagnetic pole at  $177.6^\circ\text{E}$ ,  $28.3^\circ\text{S}$ , ( $A_{95} = 12.7^\circ\text{K} = 11.6$ ). Two directional clusters of opposite inclination pass a reversal test (C-class) and the primary origin is supported by a positive baked contact test, satisfying all the seven R-criteria to provide the first West African Tonian key paleomagnetic pole. This key pole indicates a high latitude for the West Africa Craton during the emplacement of the ~860 Manso dykes. A compilation of reliable paleomagnetic poles for West Africa, Baltica, Amazonia and Congo–São Francisco cratons suggests that these cratons were together between ~1200 and 800 Ma in a long-lived WABAMGO configuration. We suggest that the collision of this block with Laurentia along the Grenvillian–Sunsás orogens closed the external Nuna Ocean and formed Rodinia by extroversion.

© 2021 International Association for Gondwana Research. Published by Elsevier B.V. All rights reserved.

## 1. Introduction

The Earth's geodynamics at the Mesoproterozoic–Neoproterozoic transition was marked by the formation of the Rodinia supercontinent, whose duration and configuration are still subject to debate (Condie, 2002; Dalziel, 1997; Evans, 2009; Hoffman, 1991; Li et al., 2013; Li et al., 2008; Meert, 2001; Meert and Torsvik, 2003; Meredith et al., 2017; Moores, 1991; Pisarevsky et al., 2003; Sears and Price, 1978;

Wen et al., 2018; Wingate et al., 2002). In all models, Laurentia is considered as the central piece of Rodinia, surrounded by passive margins during the late Neoproterozoic, similar to the African plate during the Phanerozoic (Bond et al., 1984; Hoffman, 1991). Regarding the paleomagnetic database for Rodinia, Laurentia has a substantial number of reliable paleomagnetic poles between ~1270 and 1000 Ma, but the ~1000–800 Ma interval lacks high-quality data (Evans, 2009). Around Laurentia, the models place Baltica along the northeastern coast of Laurentia/Greenland in the northern hemisphere or, as an alternative, in an inverted position (Hartz and Torsvik, 2002). Siberia is often considered to be adjacent to the northern margin of Laurentia in a range of orientations: (i) with the present-day Siberia northern margin facing the northern Laurentia margin (Dalziel, 1997; Hoffman, 1991), or (ii) in

\* Corresponding author at: Universidade de São Paulo (USP), Instituto de Astronomia, Geofísica e Ciências Atmosféricas (IAG), Rua do Matão, 1226, Cidade Universitária, 05508-090 São Paulo, SP, Brazil.

E-mail address: paulantonio0931@gmail.com (P.Y.J. Antonio).

a reverted position (Ernst et al., 2016; Rainbird et al., 1998). Paleomagnetic comparisons between Siberia and Laurentia support a relative distance between these cratons considering Siberia as a promontory of the supercontinent with smaller cratons between them (Li et al., 2008; Pisarevsky and Natapov, 2003; Pisarevsky et al., 2008). Some models have also located Siberia along the present western margin of Laurentia (Piper, 2007; Sears and Price, 1978; Sears and Price, 2000), but this position is no longer supported by paleomagnetic data (Li et al., 2008). An alternative position in the southern hemisphere near the North China Craton was also proposed (Evans, 2009). Considered as neighbors in most supercontinents (Columbia, Rodinia and Pangea), these three cratons (Laurentia–Baltica–Siberia) are defined as the “strange attractors” by Meert (2014). The Amazonia, West Africa and Rio de la Plata cratons are unconstrained by palaeomagnetic data during the ~1000–700 Ma interval, but they are usually placed in proximity to western Laurentia (Evans, 2009). Coherence between these blocks but with slight differences in orientation in different reconstructions led Meert (2014) to call them the “spiritual interlopers”. Note that at the peak of Rodinia continental assembly at ~950–850 Ma, only four continents (Baltica, São Francisco, North China, and Siberia) exhibit robust paleomagnetic data (Merdith et al., 2017). This emphasizes the still scarce paleomagnetic database for Rodinia event in its “golden age”.

The peak of continental Rodinia assembly precedes a drastic change in paleolatitude from a high-latitude for the Rodinian landmasses to a low-latitude paleogeography, which occurred at ~800 Ma, before its breakup at ~750 Ma (Li et al., 2008). This rotation began after the emplacement of a large superplume beneath the polar landmasses at ~840 Ma, triggering large magmatism and rifting (Li et al., 2003). Recently, some authors argued that these events can be better explained by a Tonian inertial interchange true polar wander (IITPW), but its amplitude, characteristics (single shift or TPW oscillations), and duration are debated (Jing et al., 2019; Li et al., 2004; Maloof et al., 2006; Niu et al., 2016; Swanson-Hysell et al., 2012). From an environmental point of view, no glacial deposits were observed in the landmasses during the polar position of Rodinia at ~950–850 Ma (Li et al., 2013), but more constraints are needed since climatic models depends strongly on the Tonian (1000–720 Ma) paleogeography (Donnadieu et al., 2004). The ~812–790 Ma interval is characterized by the Neoproterozoic Bitter Springs Anomaly (BSA), a large negative  $\delta^{13}\text{C}$  excursion which can be associated with some indicators of increasing oxygenation of the ocean and atmosphere during the radiation of early eukaryotes (Swanson-Hysell et al., 2015b).

Therefore, a precise and reliable Tonian paleogeography is crucial to understand the impact of the Rodinia supercontinent and the magmatic events it encompasses on the Earth's system. In this contribution, we performed a detailed paleomagnetic study on the ~860 Ma Manso dyke swarm (Baratoux et al., 2019) associated with new U–Pb apatite dating to obtain the first Tonian key pole for West Africa. Our first well constrained West Africa key paleomagnetic pole allows us to propose the existence of a long-lived WABAMGO juxtaposition between West Africa, Baltica, Amazonia and Congo–São Francisco cratons, which collision with Laurentia lead to the Apex of Rodina supercontinent.

## 2. Geological setting

The West African Craton is composed of two Proterozoic Shields (Reguibat Shield in the north and Leo-Man Shield in the south) stabilized at about ~2 Ga, and separated by the Upper Proterozoic–Paleozoic sedimentary Taoudeni Basin (Black et al., 1979) (Fig. 1). The Ghanaian Paleoproterozoic domain (within the Baoulé–Mossi domain) is composed of an association of granitoids and five northeastern trending greenstone belts (Bole–Nagandi, Bui, Sefwi, Ashanti, and Kibi–Winneba belts from west to east, respectively) (Feybesse et al., 2006) (Fig. 1). These greenstones and the associated sedimentary basins were deformed during the ~2100–2000 Ma Eburnean Orogeny (Bonhomme, 1962). These two Proterozoic Shields underlie

Meso-Neoproterozoic Basins (Affaton et al., 1991). The older sediments of the Volta basin (Lower Voltaian Supergroup) in southern Ghana were deposited at ~1000 Ma. The southeastern limit of the Volta basin is bordered by the Dahomeyide belt, the southern extension of the Pan-African belts (Affaton et al., 1991) (Fig. 1). These Neoproterozoic events have strongly affected the northern West African Craton, where the sedimentary sequences and dykes are folded and deformed along shear zones in the Anti-Atlas Orogen (Fig. 1) (Samson et al., 2004), while the Leo-Man Shield in turn remained stable.

Twenty-six distinct dyke swarms were identified in the West African Craton by aeromagnetic mapping according to their orientation (Jessell et al., 2015). In the Leo-Man Shield, Paleoproterozoic–Mesoproterozoic dykes are represented by the ~1790 Ma Libiri swarm, the ~1790 Korsimoro swarm, and the ~1520 Essakane swarm (Baratoux et al., 2019). Paleomagnetic poles from greenstone rocks and Paleo- to Mesoproterozoic dykes were previously reported by Piper and Lomax (1973). Two Neoproterozoic dyke swarms from Ghana were recently dated by U–Pb baddeleyite at  $915 \pm 7$  Ma for the N070° Oda dyke swarm, and  $867 \pm 16$  Ma for the N355° Manso dyke swarm (Baratoux et al., 2019) (Fig. 1). A younger generation of basaltic dykes was also recognized in the northeastern part of Ghana/southern Burkina Faso with an U–Pb baddeleyite age of  $198 \pm 16$  Ma (Hounde dyke swarm) and was related to the Central Atlantic Magmatic Province (CAMP) (Baratoux et al., 2019).

In this study, we sampled 15 dykes of the ~860 Ma NNW-trending Manso dykes and one dyke (GH07) of the ~915 ENE-trending Oda dyke swarm (Fig. 1). The Manso dykes have mainly a NNW-direction conjugated to a NNE-direction for some branches of the dyke swarm and are ~50–100 m wide (geophysical signature), but their contact with the host rock was not observed in the field. They are fresh, coarse to medium-grained dolerites composed mainly of plagioclase and clinopyroxene (augite) with Fe–Ti oxides. Rare orthopyroxene, altered olivine, baddeleyite, and sulfide were also observed (Baratoux et al., 2019). Fine-grained lamprophyre dykes containing micas and some titanite occur in the Ahafo mine. These Neoproterozoic dykes are undeformed, and they crosscut the Paleoproterozoic basement and Paleoproterozoic regional tectonic structures.

## 3. Methods

### 3.1. Sampling

Due to the dense vegetation and the occurrence of a thick (up to ~30 m) laterite cover, the outcrops of mafic dykes in Ghana are restricted to the rivers, isolated blocks (Fig. 2A, B), and fresh outcrops from mine pits. In March 2019 we sampled 121 oriented cylindrical cores using a portable gasoline-powered rock drill, as well as eight hand-samples in the Ahafo mine pit (Newmont Company), for a total of 16 sites (or dykes). According to the field orientation, 15 dykes are from the ~860 Ma NNW-trending Manso dyke swarm and one dyke (GH07) is from the ~915 Ma E-trending Oda dyke swarm (Antonio et al., 2019; Baratoux et al., 2019). The number of samples by site (5–8) were restricted essentially due to agreement with local communities and the mining company. Both cores and hand-samples were oriented using solar and magnetic compasses, and no declination difference was observed. The 16 sites sampled cover a vast geographical area (~41,500 km<sup>2</sup>) from the capital Accra in southeast Ghana to Sunyani in the northwest via Cape Coast in the south (Fig. 1 & site coordinates provided in Table 1).

### 3.2. Geochronology

Two samples (GH05 and GH16) were selected for U–Pb geochronology on apatite. Apatite separation was performed in the Géosciences Environnement Toulouse (GET, France) laboratory. Hand-samples were crushed and sieved to collect the mineral fraction below 400 µm. The

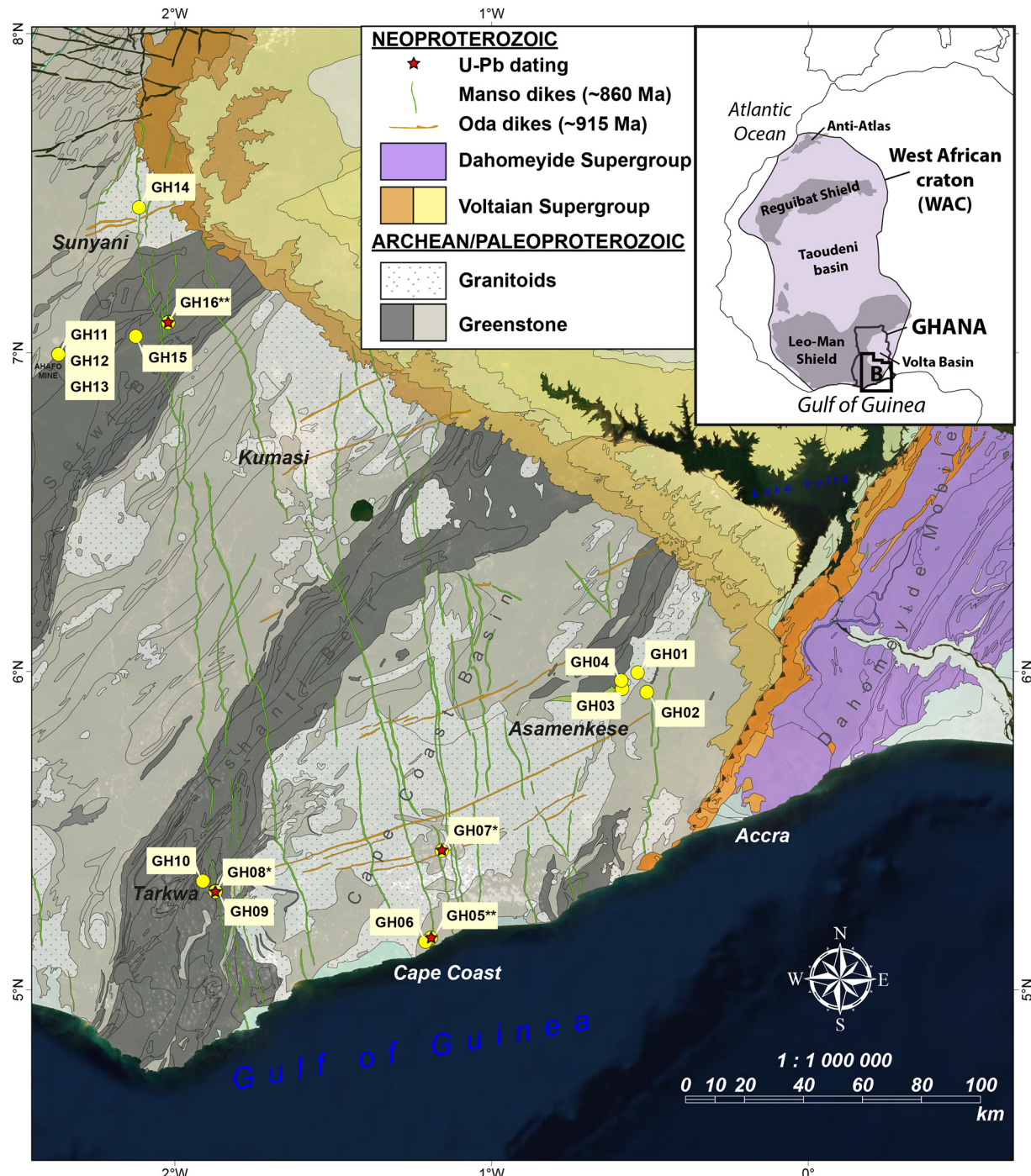


**Fig. 1.** Inset: Location of the study area in the West African Craton (WAC). Geological map of the Neoproterozoic units of Ghana with sampling location for geochronology (red stars) and paleomagnetism. \*: U–Pb baddeleyite age of GH08 =  $867 \pm 16$  Ma (Manso) and GH07 =  $915 \pm 7$  Ma (Oda) from Baratoux et al. (2019). \*\*: U–Pb apatite ages of GH05 =  $857.2 \pm 8.5$  Ma and GH16 =  $855 \pm 16$  Ma from this study.

low-density minerals and clay fraction were removed using a Wilfley table. Heavy minerals were then isolated using heavy liquids (tetrabromoethane and diiodomethane, with respective densities of 2.967 and 3.325 g/cm<sup>3</sup>). Magnetic minerals were consequently removed with a Franz magnetic separator. Finally, the apatite grains were handpicked using a binocular microscope before being mounted into epoxy puck and polished. U–Pb data were acquired at the Isotopic Geochemistry Laboratory in Federal University of Ouro Preto (UFOP, Brazil) using a 193 nm HelEX Photon Machine coupled with a ThermoScientific Neptune Plus Multicollector (LA-MC-ICP-MS).

A beam spot size of 85 µm was used with beam energy densities of 6 J/cm<sup>2</sup>, and a 6-Hz repetition rate. During apatite U–Pb measurement sequences, the 91,500 zircon (Wiedenbeck et al., 1995) was used as a primary reference standard, while the Durango apatite (McDowell et al., 2005), the 401 apatite (Thompson et al., 2016), and the Madagascar apatite (Thomson et al., 2012) were used as secondary reference material in order to correct for matrix match effects as well as to constrain and verify the corrections accuracy and reproducibility. Data reduction and correction was carried out with the SATURN package of the laboratory of Ouro Preto. Apatite U–Pb ages of the studied

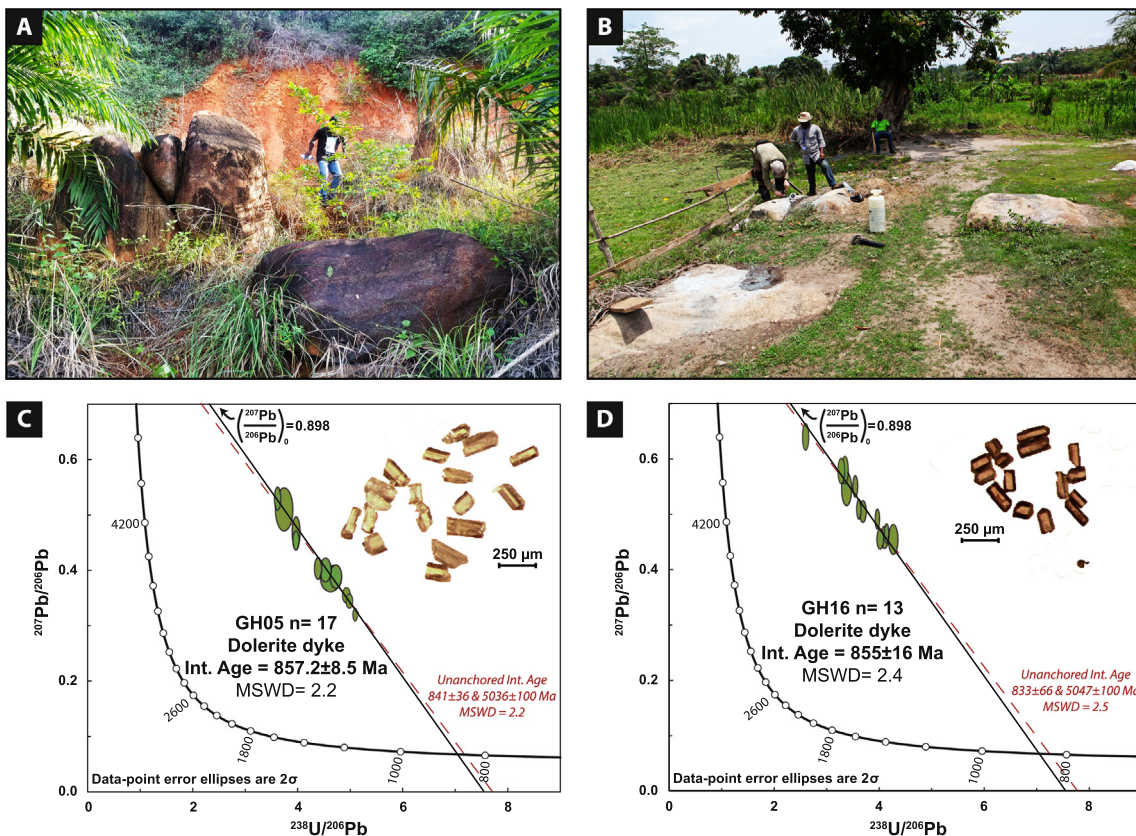


**Fig. 2.** A and B: Field photographs of the Manso dolerite dykes at GH05 and GH16 sites, respectively. C and D: U–Pb Terra-Wasserburg diagrams for apatite dating of the Manso dolerite dykes at GH05 (C) and GH16 (D) sites. The upper intercept is anchored to the initial Pb/Pb ratio (0.898) that was calculated based on Pb model of Stacey and Kramers (1975) for an emplacement age of ~867 Ma (Baratoux et al., 2019). Unanchored ages are also illustrated (in red).

samples are reported as isochron ages calculated as lower-intercepts on a Terra-Wasserburg Concordia diagram using the Isoplot 4.15 software (Fig. 2) (Ludwig, 2009). The grains analyzed from each sample are igneous co-genetic apatites. Initial common Pb value was anchored to a  $^{207}\text{Pb}/^{206}\text{Pb}$  value of 0.898 (Stacey and Kramers, 1975) according to the U–Pb baddeleyite (ID-TIMS) crystallization age of  $867 \pm 16$  Ma (Baratoux et al., 2019). All the apatite isotopic data, at  $2\sigma$  level, are reported in the supplementary material 1. Additional information on the analytical conditions, and the Terra-Wasserburg Concordia diagrams of reference materials, are provided in the supplementary material 2.

### 3.3. Paleomagnetism

Oriented blocks were drilled in Geosciences Montpellier (France). Preparation of standard specimens (2.2 cm height) and alternating field (AF) demagnetization for a pilot study were carried out at the GET (Toulouse, France) using a JR5-A spinner magnetometer and a LDA-3 AF demagnetizer (AGICO) in a MMLFC shielded room design to reduce the effect of ambient magnetic field (<200 nT). For the remaining samples, the characteristic remanent magnetization (ChRM) was isolated by stepwise AF and thermal demagnetization performed in a magnetically shielded room with ambient field <500 nT at the Laboratorio de Paleomagnetismo of the University of São Paulo (USPMag, Brazil). An AF pre-treatment until 10 mT was performed before thermal demagnetization, to eliminate an eventual low-coercivity, viscous component. AF and thermal demagnetizations were performed using a vertical 2G-Enterprises™ DC-SQUID magnetometer with a RAPID automatic sample changer (Kirschvink et al., 2008). Stepwise thermal demagnetization of 50 °C (until 500 °C) and 20 °C (until 700 °C) were carried out using a TD-48 furnace device. Only principal

component analysis (PCA) (Kirschvink, 1980) was used to determine the remanence directions using orthogonal vector diagrams (Zijderveld, 1967). Site mean directions and paleomagnetic poles were calculated by Fisher's (1953) statistics using the PALEOMAC package (Cogné, 2003). Paleogeographic reconstructions were performed using the GPlates software (Müller et al., 2018). Magnetic mineralogy was investigated under optical microscopy and using a Scanning Electron Microscopy (SEM JEOL JSM 7100F TTLS LV – EDS/EBSM) at the Centre de Micro Caractérisation Raimond Castaing (Toulouse, France). High-temperature thermomagnetic curves (susceptibility versus temperature) were conducted at the Toulouse, France in an argon atmosphere using a CS-3 apparatus coupled to the KLY-3 Kappabridge (AGICO, Brno, Czech Republic). In addition, hysteresis loops, isothermal remanent magnetization (IRM) and first-order reversal curve (FORC) for selected samples were performed at the LABGeo, Instituto Oceanográfico, University of São Paulo (Brazil) using a MicroMag-VSM, Model 3900 (Princeton Measurements Corporation). FORC diagrams were processed using the Forcot software (Berndt and Chang, 2019).

## 4. Results

### 4.1. Geochronology

The GH05 site is situated near Cape Coast, between the towns of Yamoransa and Biriwa (southern Ghana) (Fig. 1). It is a 20–50 m wide dyke disintegrated into several blocks of coarse-grained relatively fresh dolerite, with ~0.5 cm of weathering crust (Fig. 2A). The second dated site GH16 is located within the Bechem city (SE of Sunyani) (Fig. 1). Multiple blocks of metric size (*in situ*) were observed in an

**Table 1**

S.lat, S.lon are the site latitude and longitude. n/N - number of specimens used in mean directions/number of analyzed specimens; Dec – Declination; Inc. – Inclination; R – the resultant vector,  $\alpha_{95}$  (A95) is the radius of the 95% cone of confidence and k (K) is the precision parameter - Fisher's statistical parameters (Fisher, 1953) for the mean directions (*mean virtual geomagnetic poles – VGPs*); P.Lat – pole latitude; P.Long – pole longitude. Values of mean sites directions are indicated in bold for the positive, negative, and combined polarities. \*: U-Pb baddeleyite age of GH08 =  $867 \pm 16$  Ma (Manso) and GH07 =  $915 \pm 7$  Ma (Oda) from Baratoux et al. (2019). \*\*: U-Pb apatite ages of GH05 =  $857.2 \pm 8.5$  Ma and GH16 =  $855 \pm 16$  Ma from this study.  $\gamma_c$ : Site with an attempted baked contact test (BCT).  $\gamma$  ( $\gamma_c$  = critical) is the angle calculated between the mean directions of reversed and normal polarities (McFadden and McElhinny, 1990).

Sites (Samples)	S.lat (°N)	S.lon (°E)	Lithology	Characteristic remanent magnetization (ChRM)						VGP	
				n/N	Dec (°)	Inc (°)	R	k	$\alpha_{95}$ (°)	P. Lat (°N)	P. Long (°E)
<b>Cluster (A+) with downward inclination (positive)</b>											
GH03 (A-O)	5.946	359.413	Dolerite dyke, medium to coarse grained	30/40	22.6	51.8	29.07	31	4.8	55.3	33.8
GH11 (OB1-OB2)	6.994	357.633	Lamprophyre dyke	13/13	320.6	86.7	12.91	314.8	3.6	11.1	352.7
GH12 (OB3-OB4)*	6.994	357.633	Lamprophyre dyke	14/17	87.9	86.8	13.87	100.2	4	6.2	3.4
GH13 (OB5)	6.994	357.633	Lamprophyre dyke	14/14	82.1	88.2	13.98	548	1.7	6.5	0.6
GH15 (A-H)	7.051	357.876	Dolerite dyke, fine to medium grained	6/8	3.7	63.9	5.93	77.2	7.7	51.3	1.2
<b>Mean positive polarity</b>				<b>5 sites</b>	<b>16.6</b>	<b>76.7</b>	<b>4.81</b>	<b>21</b>	<b>17.1</b>	<b>26.4</b>	<b>3.9</b>
							<b>R = 4.54</b>	<b>K = 8.7</b>	<b>A95 = 27.5</b>		
<b>Cluster (A-) with upward inclination (negative)</b>											
GH01 (A-L)	5.996	359.462	Dolerite dyke, medium grained	9/24	207.6	-57.2	8.6	20	11.8	-49.5	213.3
GH02 (A-H)	5.935	359.490	Dolerite dyke, medium grained	11/28	220.2	-70.9	10.72	35.6	7.8	-31.2	205
GH05 (A-H)	5.163	358.809	Dolerite dyke, medium grained**	10/15	137.6	-85.2	9.84	57.8	6.4	-11.9	171.5
GH08 (A-H)	5.309	358.130	Dolerite dyke, medium grained*	17/17	136.9	-78.2	16.99	1134	2.4	-21.2	161.5
GH09 (A-F)	5.307	358.129	Dolerite dyke, medium grained	9/12	142.2	-72.3	8.89	67.2	6.3	-29.8	155.7
GH10 (A-E)	5.341	358.088	Dolerite dyke, fine grained	8/19	127.8	-68.8	7.81	37.4	9.2	-26.3	145.3
GH14 (A-F)	7.454	357.887	Dolerite dyke, medium grained	12/15	152.7	-80.4	11.97	338.6	2.4	-23.5	167.8
GH16 (A-K)	7.095	357.979	Dolerite dyke, coarse grained**	12/22	198.1	-78.6	11.94	168.4	3.4	-27.7	184.5
<b>Mean negative polarity</b>				<b>8 sites</b>	<b>172.8</b>	<b>-77</b>	<b>7.81</b>	<b>37.1</b>	<b>9.2</b>	<b>-29.2</b>	<b>173.7</b>
							<b>R = 7.47</b>	<b>K = 13.2</b>	<b>A95 = 15.8</b>		
<b>MEAN MANSO POLE - COMBINED (by sites)</b>											
<b>Angles of reversal test</b>				<b>13 sites</b>	<b>181.9</b>	<b>-77.2</b>	<b>12.6</b>	<b>30.6</b>	<b>7.6</b>	<b>-28.3</b>	<b>177.6</b>
<i>Mean combined (by specimens)</i>							<b>R = 11.97</b>	<b>K = 11.6</b>	<b>A95 = 12.7</b>		
<i>Mean secondary (by site)</i>				165	187.9	-75.9	156.6	19.6	2.5		
				10 sites	357.7	1.3	9.23	11.7	14.7	84.3	197.8
<i>Sites not considered in the Manso pole.</i>											
GH04 (A-U)	5.971	359.409	Dolerite dyke, medium grained (not <i>in situ</i> )	34/35	114.6	13.5	33.12	37.7	4.1	-23.5	79.3
GH06 (A-E)	5.150	358.792	Dolerite dyke, fine grained (not <i>in situ</i> )	8/12	330	23.8	7.65	20	12.7	59.4	284.1
GH07 (A-H)	5.436	358.843	Dolerite dyke, fine grained (-915 Ma)*	28/29	245.3	-62.7	26.99	26.7	5.4	-21.1	222.3
<i>Baked contact test</i>											
Mean baked - BCT (GH12)	6.994	357.633	Foliated granodiorite	9/11	117.9	80.3	8.93	112.8	4.9	-2.9	13.6
Mean unbaked - BCT (GH12)	6.994	357.633	Foliated granodiorite	9/14	291.3	31	8.83	46.7	7.6	22.1	282.7

open area (Fig. 2B). The dyke is a coarse-grained dolerite showing a fresh doleritic texture (*i.e.* intergranular subophitic).

Apatites from the doleritic samples (GH05 and GH16) exhibit a nearly perfect euhedral prism shape (Fig. 2C, D) with grain size ranging between 90 and 300  $\mu\text{m}$ . The isotopic data obtained for the GH05 dolerite sample displays variable proportions of common Pb with  $^{207}\text{Pb}/^{206}\text{Pb}$  values varying between 0.32 and 0.53. The anchored lower intercept age for this sample is  $857.2 \pm 8.5$  Ma with a MSWD of 2.2 using 17 apatites (Fig. 2C). Sample GH16 (dolerite dyke) displays variable proportions of common Pb with  $^{207}\text{Pb}/^{206}\text{Pb}$  values between 0.45 and 0.64. Data for this sample define an anchored lower intercept age of  $855 \pm 16$  Ma with a MSWD of 2.4 using 13 apatites (Fig. 2D). The unanchored plots give identical ages for GH05 and GH16 respectively within the error of  $841 \pm 31$  Ma (MSWD = 2.2) and  $833 \pm 66$  Ma (MSWD = 2.5), respectively, but the anchored ages were preferred following Chew et al. (2011).

#### 4.2. Paleomagnetic results

Natural remanent magnetization (NRM) values for the dolerite dykes vary between  $\sim 0.1$  and  $9.8 \text{ A.m}^{-1}$ . Samples showing scattered NRM directions and higher intensity values of  $270\text{--}555 \text{ A.m}^{-1}$  (*e.g.* GH07A, B) were discarded, most probably due to lightning effects.

A stable magnetic component was reached for the NNW-trending Manso dolerite dykes after removing a secondary/viscous component. Linear behavior is generally observed with two well-defined segments in the Zijderveld plots with a “high coercivity/temperature component” revealed above AF values of 17 mT (Fig. 3A, E, and F) and temperature values range of  $\sim 540\text{--}580$  °C (Fig. 3B, C, and D). These unblocking temperatures ( $T_{ub}$ ) point toward magnetite as the main carrier of the high-temperature component. Calculated by PCA analysis, a characteristic remanent magnetization (ChRM) is revealed for a first cluster (A+) of five sites showing a northern direction with a positive inclination (Fig. 3A, B). A second cluster (A-) is composed of eight sites with a ChRM of southern direction with a steep negative inclination (Fig. 3C, D, and E).

Most low coercivity-temperature components yield northern directions with shallow inclinations with the subsequent secondary site-mean direction is  $D_m = 357.7^\circ$ ,  $I_m = 1.3^\circ$  ( $\alpha_{95} = 14.7^\circ$ ,  $k = 11.7$ ), close to the present dipolar field (PDF) (Fig. 4A). Three sites (GH03, GH10, GH14) show a different secondary direction of north-western directions.

A total of 165 specimens (13 sites) was used to calculate the Manso pole using the high coercivity-temperature components. Using the sites with positive inclinations ( $D_m = 16.6^\circ$ ,  $I_m = 76.7^\circ$ ,  $n = 5$ ,  $k = 21$ ) and the sites with negative inclinations ( $D_m = 172.8^\circ$ ,  $I_m = -77^\circ$ ,  $n = 8$ ,  $k = 37.1$ ), the Manso dyke swarm passes a reversal test with a critical

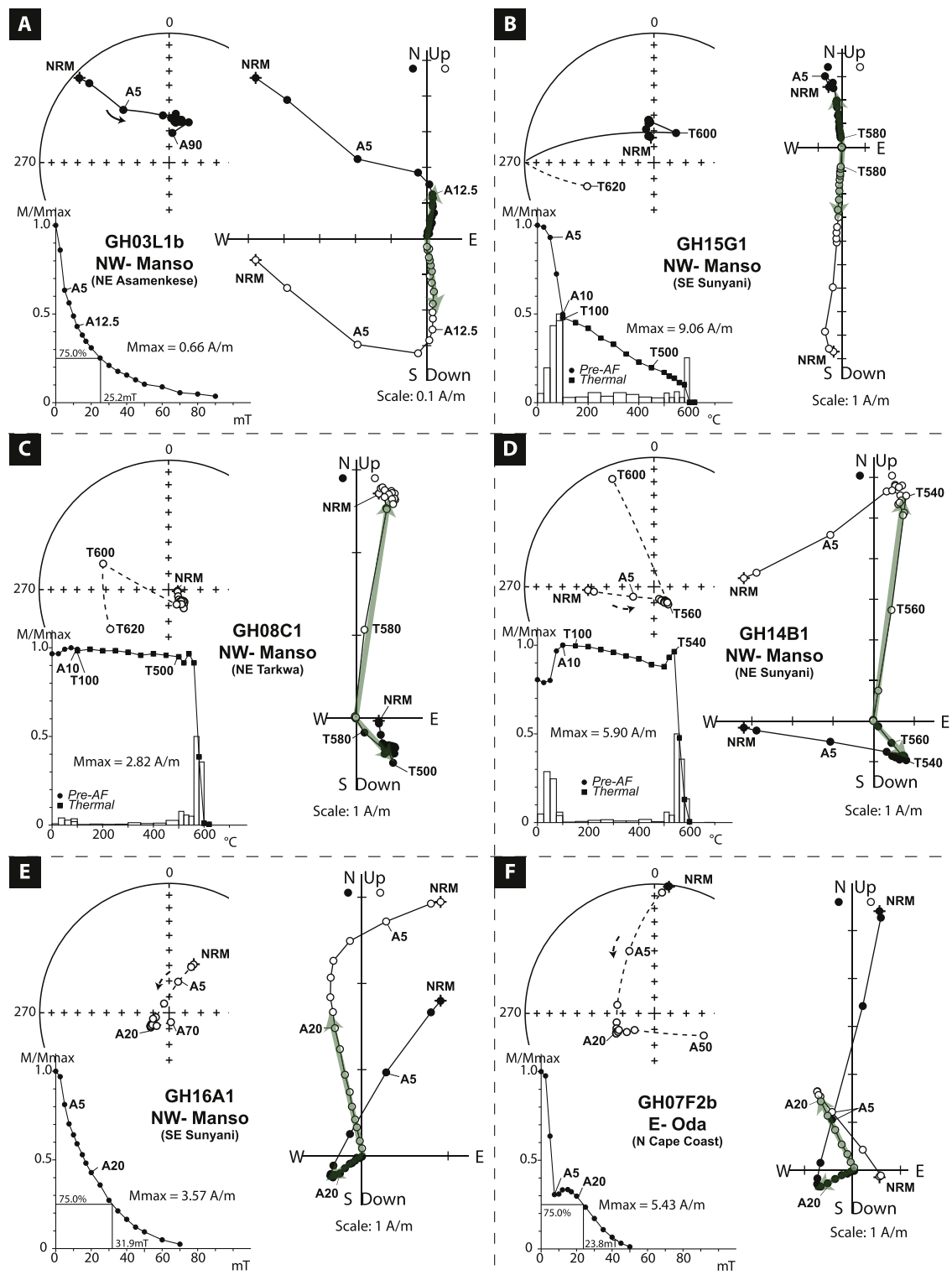


**Fig. 3.** Representative demagnetization plots of Neoproterozoic dykes for different geographic sites in Ghana after AF and thermal demagnetizations. Equal-area stereonet (filled (open) symbols represent positive inclination), Zijderveld plots (vertical/horizontal projections shown by open/filled circles), and Magnetization intensity decay curves ( $M/M_{\text{max}}$ ) are indicated for each example. Values of 75% of the NRM decay (in mT) and unblocking temperature spectra are indicated for the AF and thermal demagnetization curves, respectively. NRM = natural remanent magnetization. Numbers, T100 (A5), indicate thermal (AF) demagnetization step. NRM = natural remanent magnetization. Numbers, T100 (A5), indicate thermal (AF) demagnetization step.

gamma of  $16.2^\circ$  and a difference of  $5.4^\circ$  between normal and reverse axes (reversal test of C-class) (McFadden and McElhinny, 1990). The Manso pole (13 sites) was calculated using the 5 sites of positive inclinations and the 8 sites of negative inclinations (Fig. 4C) giving a site mean direction of  $D_m = 181.9^\circ$ ,  $I_m = -77.2^\circ$  ( $\alpha_{95} = 7.6^\circ$ ,  $k = 30.6$ ),

yielding to a paleomagnetic pole located at  $28.3^\circ\text{S}$  and  $177.6^\circ\text{E}$  ( $A95 = 12.7^\circ\text{K} = 11.6$ ) (Table 1; Fig. 4C, D).

An iterative cutoff of  $37.6^\circ$  was determined using the 13 sites with no site exclusion (Vandamme, 1994), yielding a VGP dispersion ( $S$ -value) of  $23.8^\circ$  (Fig. 4D). High dispersion is expected for results with high

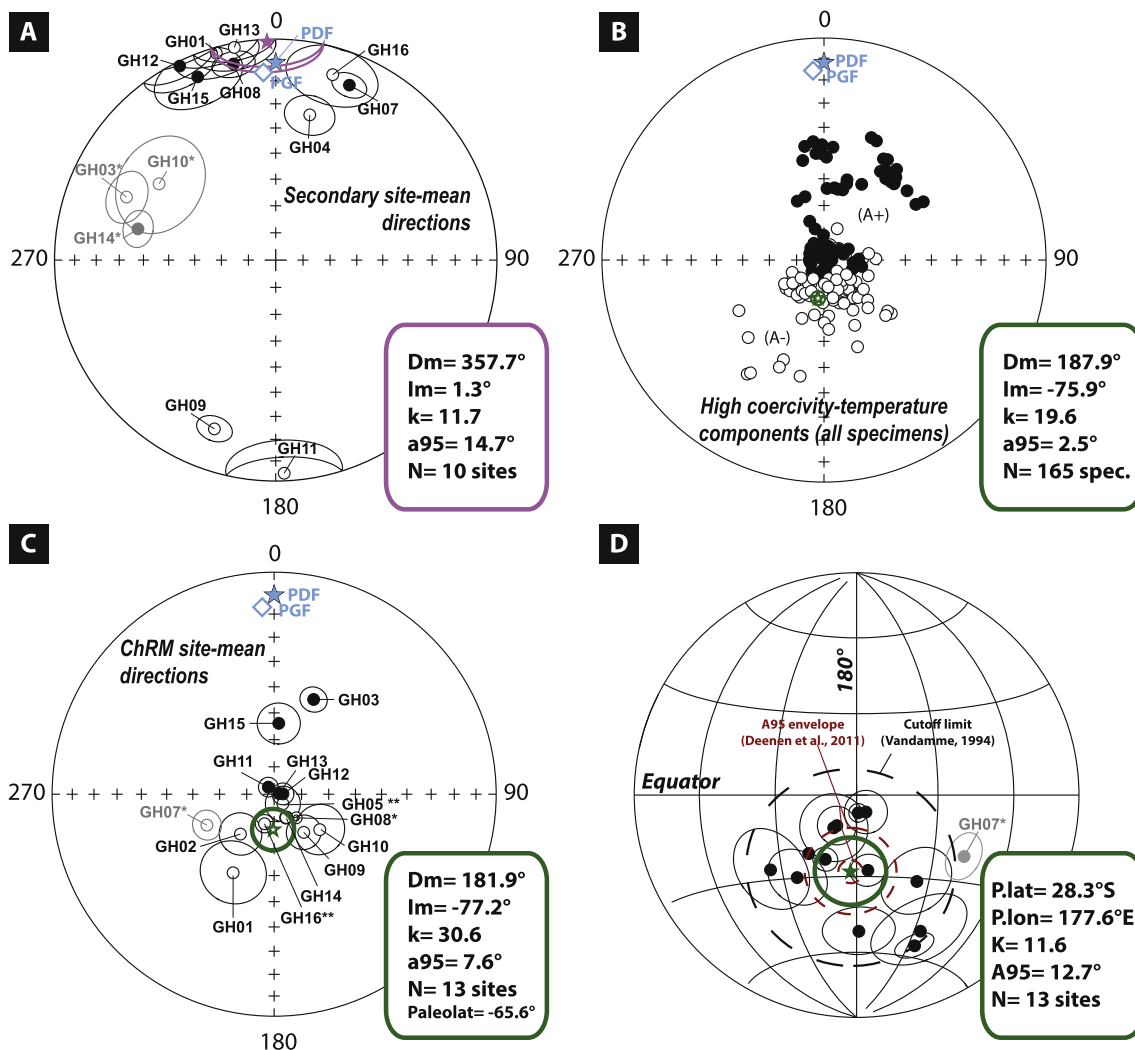


**Fig. 4.** Sample and site mean directions for the Manso dykes. A: Secondary site-mean directions calculated from the low coercivity/temperature components (\*: not considered in the mean secondary directions). B: Specimen mean directions of the high coercivity/temperature components (in green). C: Site mean directions for the Manso dykes (in green). Sites/specimens with positive and negative inclinations are represented with filled (open) symbols represent downward (upward) inclinations. Confidence circle ( $\alpha 95$ ) around the means are indicated. PDF – Present dipolar geomagnetic field; PGF – Present geomagnetic field. D: Dispersion of site mean virtual geomagnetic poles (VGPs) and paleomagnetic pole calculated for the Manso dykes (Table 1) represented in a Schmidt projection. Deen et al. (2011)'s A95 envelope (4.3°–16.3°) and the iterative cutoff limit (37.6°) of Vandamme (1994) are indicated. \*: U–Pb baddeleyite age of GH08 = 867 ± 16 Ma (Manso) and GH07 = 915 ± 7 Ma (Oda) from Baratoux et al. (2019). \*\*: U–Pb apatite ages of GH05 = 857.2 ± 8.5 Ma and GH16 = 855 ± 16 Ma from this study. Direction and VGP for the ~915 Ma site (GH07) are indicated in grey, not considered for the Manso pole.

inclination values as suggested by paleosecular models of latitudinal dependence of S (e.g. Model-G from McFadden et al. (1988)). The A95 for the Manso pole is equal to 12.7° which is comprised within the A95 envelope (4.3°–16.3°) of Deen et al. (2011) (see Fig. 4D). Altogether, these characteristics suggest that our sampling of the Manso dolerite dykes average the paleosecular variation.

Though based on a single site (GH07), a stable ChRM of steep negative inclination and southwestern direction was obtained for the ~915 Ma E-trending Oda dyke, similar to the A-cluster of the Manso dykes (Fig. 3F) providing a VGP at 21°S and 222.3°E.

#### 4.3. Baked contact test

Due to the weathering cover, host rocks could only be sampled in the Ahafo mining pit (Newmont Company) in the Sefwi Belt (Fig. 5), to attempt a baked contact test (BCT). Fig. 5A shows the sampled outcrop where two undeformed lamprophyre dykes (GH11 as illustrated in Fig. 5B, and GH12) are cutting the granodiorite host rock deformed

during the ~2000 Ma Eburnean orogeny (Feybesse et al., 2006). Two oriented blocks (OB3 and OB4) were collected for the GH12 dyke (Fig. 5A). To attest the primary origin of the magnetization carried by the dyke GH12, we sampled one oriented block (OB6) within the baked zone into a two-branched dyke. The oriented blocks OB7 and OB8 were sampled at ~1 m and ~30 m respectively from the GH12 dyke. Thermal demagnetizations revealed a high unblocking temperature interval ( $T_{ub}$ ) of 520–620 °C and high stability for the ChRM of the baked host rock at the contact (OB6) with a site-mean of  $D_m = 117.9^\circ$  and  $I_m = 80.3^\circ$  ( $\alpha 95 = 4.9^\circ$ ,  $k = 112.8$ ) (Table 1; Fig. 5C, D). The host rock at the contact shows the same ChRM direction of the GH12 dyke ( $D_m = 87.9^\circ$ ,  $I_m = 86.8^\circ$ ,  $\alpha 95 = 4^\circ$ ,  $k = 100.2$ ) (Table 1; Fig. 5C, D). The secondary components are close to the present field with a northwestern direction and a low inclination for the dyke and the host rock. At ~1 m from the dyke, the OB7 block shows a significantly different behavior where thermal and AF demagnetizations reveal a more unstable magnetization (Fig. 5C), nevertheless magnetic vectors were defined for this block with two specimens providing a direction close to the dyke's direction

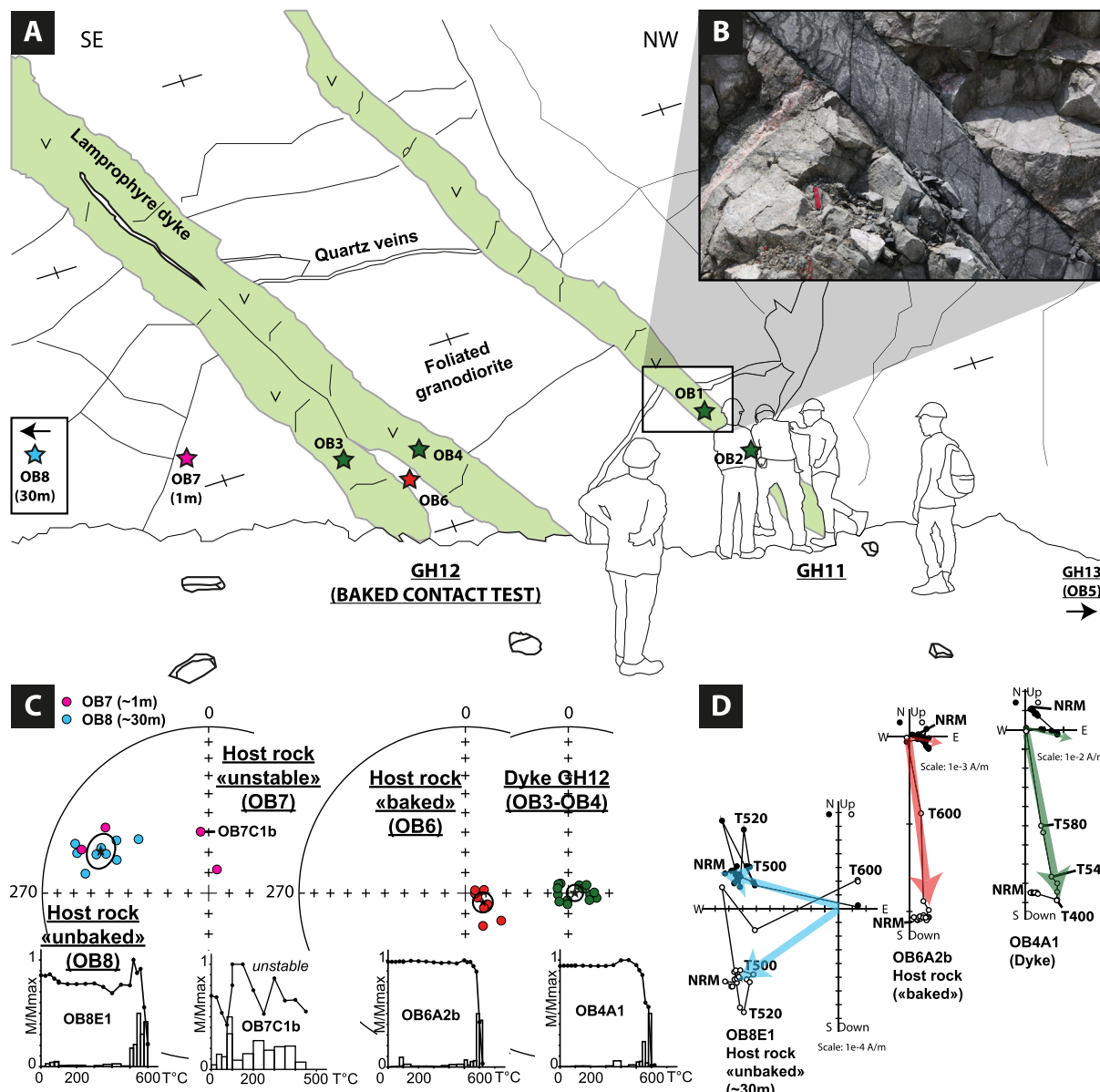


**Fig. 5.** Baked contact test for the GH12 dyke (~1 m in width). A: Geological sketch of the outcrop with location of the sampled oriented blocks (star) of dykes (in green), and the host rocks at contact (in red), at ~1 m (in pink), and at ~30 m (in blue) from the contact. B: Field photograph of the GH11 lamprophyre dyke, 0.30 m wide, located in (A). C: Equal-area stereonets (filled (open) symbols represent positive inclination) of site-mean directions for the GH12 dyke (in green) and the subsequent host rocks at contact (in red), at ~1 m (in pink), and ~30 m (in blue) from the contact. Magnetization intensity decay curves ( $M/M_{\text{max}}$ ) are indicated. D: Zijderveld plots for representative specimens after thermal demagnetization from the GH12 dyke (OB4A1), the host rock at contact (OB6A2b) and at ~30 m (OB8E1).

and two specimens showing a western direction with low positive inclination (Fig. 5C). This western direction was also disclosed for the oriented block collected at ~30 m from the contact (OB8). Differently from the OB7 block, specimens from the OB8 block are well-clustered ( $D_m = 291.3^\circ$ ,  $I_m = 31^\circ$ ,  $\alpha_{95} = 7.6^\circ$ ,  $k = 46.7$ ) with a stable ChRM until ~500 °C. This baked contact test can be considered as positive and attests to the primary origin of the stable ChRM disclosed in the Manso dykes.

#### 4.4. Magnetic mineralogy

Most opaque phases show composite texture of ilmenite-magnetite and probably titanomagnetite (Haggerty, 1991). Fig. 6A shows a representative magnetite with ilmenite lamellae in a coarse-grained dolerite dyke (GH16). Intergrowth textures with ilmenite exsolutions are

generally related to a stable thermoremanent magnetization (TRM) which supports our interpretation of the paleomagnetic results (Evans and Wayman, 1974). Fig. 6B shows three thermomagnetic curves, two for the Manso (GH08 and GH14) and one for the Oda dyke (GH07). The sample GH08A shows a curve with a reversible behavior between the heating and cooling steps whereas the cooling curve for samples GH14B3 and GH07B3 are not perfectly reversible. All samples show a Curie temperature ( $T_c$ ) at about 560–580 °C, and a Hopkinson peak for GH08 and GH14 just below  $T_c$  (Dunlop, 1974), characteristic of fine-grained pure magnetite. The Day plot (Fig. 6C) and FORC diagrams (Fig. 6D) indicate domain states mainly in the stable single-domain (SD) to pseudo-single domain (PSD) fields. Values of Mrs./Ms. higher than 0.10, and the strong proportion of 60–40% of single domains magnetite in the Day plot are consistent with the narrow unblocking temperatures above 540 °C. FORC diagram of sample GH08H1 is typical of

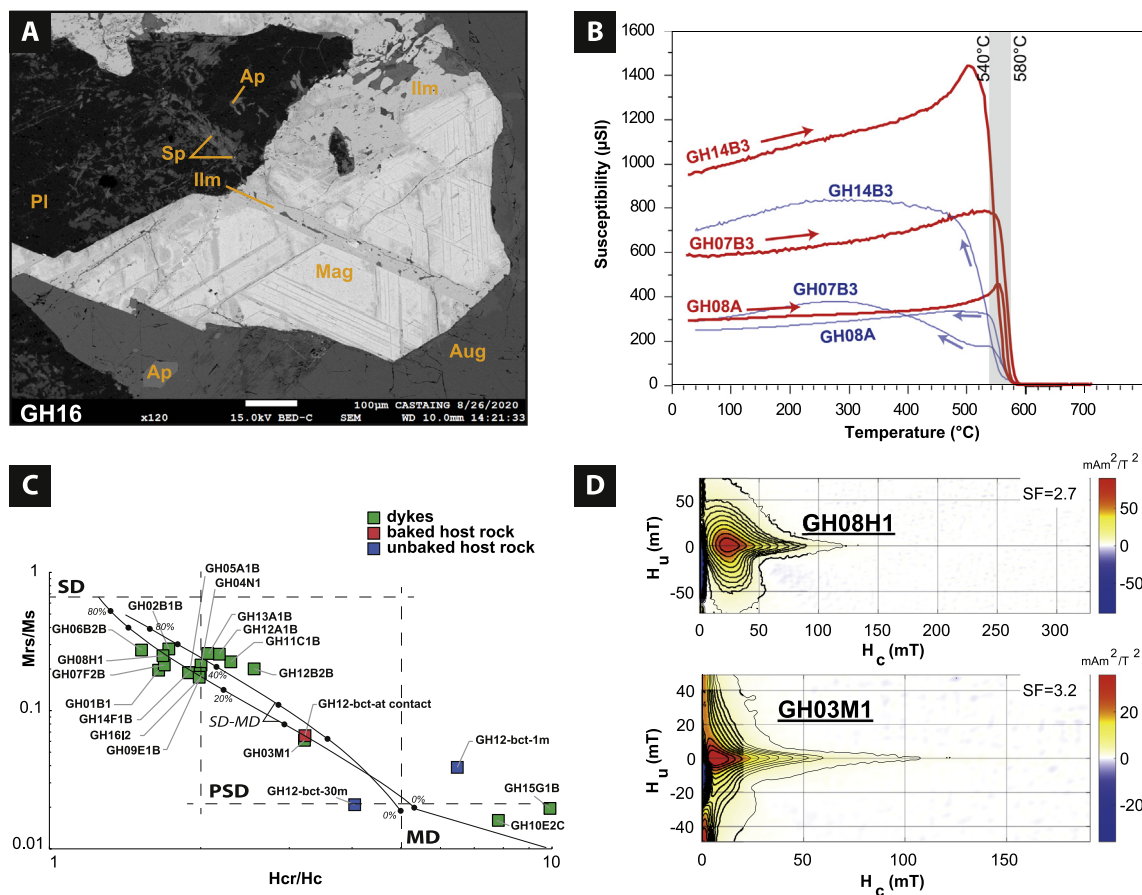


**Fig. 6.** A: SEM-BSE micrograph of titanomagnetite (Mag) with exsolutions of ilmenite (Ilm), augite (Aug), plagioclase (Pl), sphalerite (Sp), and apatite (Ap) for the GH16 dyke. B: Heating (in red) and cooling (in blue) thermomagnetic curves for three samples (GH14B3, GH07B3, and GH08A). C: Day plot for the Manso dykes and the host rocks with SP-MD mixture lines indicating the single domain proportions. SD: single domain, PSD (or vortex state): pseudo-single domain, MD: multidomain. D: First-order reversal curve (FORC) diagrams for the GH08H1 and the GH03M1 specimens. SF is the smoothing factor used by the FORCOT software.

the PSD behavior (Roberts et al., 2014), with SD-like magnetite dominance of the magnetic assemblage as shown by the peak value of ~25 mT with closed contours on the  $H_u = 0$  axis (Fig. 6D). Conversely, the GH03M1 sample show a strong proportion of multi-domain (MD) grains mixed with SD grains as suggested by a large coercivity distribution on the  $H_u$  axis. This SD/MD behavior is also confirmed by the position of GH03M1 in the Dunlop (2002) mixing curves of the Day plot (Fig. 6D). GH15 sample fall in the MD field of the Day diagram which suggests a strong proportion of MD-like magnetite in the magnetic assemblage, consistent with the strong decay of ~50% of its NRM at 10 mT during AF pre-treatment (Fig. 3B). The host rocks fall into the PSD domain for samples at the contact, whereas samples far from the contact fall into the MD field of the Day plot (Fig. 6C), suggesting a less stable behavior for these rocks. This further confirms that the host rock at the contact was mineralogically affected and re-heated during the dyke's intrusion.

## 5. Discussion

### 5.1. Reliability of the Manso paleomagnetic pole (R-criteria)

The Manso paleomagnetic pole was calculated with 13 sites of NNW-trending mafic dykes in Ghana and satisfies all seven criteria of the revised "R" reliability index (Meert et al., 2020). (R1) The Manso dyke swarm is well-dated by multi-method radiometric dating with one U-Pb baddeleyite (ID-TIMS) age of  $867 \pm 16$  Ma ( $^{207}\text{Pb}/^{206}\text{Pb}$

weighted mean age) (GH08) (Baratoux et al., 2019) and two identical (within error) U-Pb apatite ages of  $857.2 \pm 8.5$  Ma (GH05) and  $855 \pm 16$  Ma (GH16) (Fig. 2). Given that the U-Pb apatite system (Chew and Spikings, 2015) has a lower closure temperature (550–350 °C) than the U-Pb baddeleyite system (700–1100 °C) (Heaman and LeCheminant, 2001), these identical ages within error suggest the U-Pb apatite system recorded the age of crystallization. Using the U-Pb baddeleyite  $^{207}\text{Pb}/^{206}\text{Pb}$  weighted mean age of  $867 \pm 16$  Ma (or the Concordia age:  $855 \pm 10$  Ma) (Baratoux et al., 2019) combined with the two new U-Pb apatite ages, a mean age of  $858.6 \pm 6.7$  ( $856.1 \pm 6$ ) Ma can be calculated for the emplacement of the NNW-trending Manso dyke swarm. (R2) ChRM directions were isolated on 13 sites (165 specimens) by thermal and AF demagnetizations and no difference was observed between the two demagnetization methods. Moreover, all vectors were well-defined by stable linear segments reaching the origin (Fig. 3), and analyzed by PCA analysis using Zijderveld plots and equal-area projections (Kirschvink, 1978; Zijderveld, 1967). Our new Manso pole is characterized by a value of precision K of 11.6, above the lower limit of 10 proposed by (Meert et al., 2020). In addition, the A95 of 12.7° is comprised within the Deenen et al. (2011)'s interval (4.3°–16.3°) showing that the pole averages the paleosecular variation (Fig. 4D). No VGPs were excluded by the iterative cutoff of Vandamme (1994). (R3) The magnetic properties of these mafic dykes confirm their remanent magnetization is carried by a magnetic assemblage dominated by SD-like magnetite (Fig. 6). (R4) A positive baked contact test for the GH12 dyke confirms the remanence

is primary. In addition, a primary origin is also suggested by the narrow and high unblocking temperatures ( $T_{ub}$ ) (540–580 °C) of the Manso dykes which are above those of the undisturbed U—Pb apatite system (550–350 °C). (R5) These undeformed dykes were sampled in a vast geographic area in Ghana considered as stable and without evidence of deformation related to the Pan-African belts or younger tectonic events. Moreover, geochronological and paleomagnetic results of distant sites (e.g. between GH05 and GH16, which are 233 km apart from each other) support a strong regional consistency in our results. The younger events in the area were associated with the magmatic activity of the Central Atlantic Magmatic Province (CAMP) and the Atlantic rifting between Africa and South America (Baratoux et al., 2019). These events produced a low-temperature regional influence of <120 °C (Fernie et al., 2018), not sufficient to affect the primary magnetization of the dykes. This could be consistent with the secondary components of northwestern directions with shallow inclinations obtained for most of dykes that are close to both the present dipolar field and the directions obtained for the CAMP magmatism from West Africa (Palencia-Ortas et al., 2011) (Fig. 4B). (R6) The Manso pole passes a reversal test (McFadden and McElhinny, 1990) with 5 sites of positive inclination and 8 sites of negative inclination. (R7) The A95 envelope of Manso pole overlaps the robust B2 group ( $R = 6$ ) of Robert et al. (2017) for volcanic units of ~550–530 Ma sampled in the Anti-Atlas mountains, north of the West African Craton. Nevertheless, Meert et al. (2020) underline that comparison to younger poles should be discarded if the younger poles come from an orogenic belt, which is the case with the B2 pole, calculated from units folded during the Carboniferous–Permian Hercynian (or Variscan) orogeny (Robert et al., 2017). Therefore, a remagnetization of the Manso dykes seems improbable because no evidence of deformation has been documented in the study area, and our large spatial sampling discard any localized tectonic rotations. Thus, we can consider that the Manso pole fulfills all the R7 criteria of Meert et al. (2020). The ~860 Ma Manso paleomagnetic pole can thus be considered as a high-quality key pole and can serve as the first Neoproterozoic reference for the paleogeography of West Africa during Rodinia.

## 5.2. Testing the existence of the long-lived WABAMGO configuration in Rodinia

The Grenville, Sveconorwegian, and Sunsás orogens are typically used to reflect the collision between Laurentia, Baltica and Amazonia between ~1200 and 1000 Ma assembling the Rodinia supercontinent (Hoffman, 1991). This combination between these cratons is nearly identical in several Rodinia reconstructions but was questioned by Meert and Torsvik (2003), and more recently by Evans (2009) using an updated paleomagnetic database. Recently, Martin et al. (2020) re-evaluated the isotopic signature of the long-lived Paleo- to Mesoproterozoic accretionary orogens along the margins of Laurentia, Baltica, Amazonia, and Kalahari. In their model, the core of Rodinia is defined by the Laurentia–Baltica–Amazonia–Kalahari connection finally sutured during the Stenian. In the Rodinian reconstructions, West Africa is still associated with the Amazonia Craton but this link is unconstrained by paleomagnetic data during the Neoproterozoic (D’Agrella-Filho et al., 2016). Using the Manso pole, we can test if a long-lasting connection is paleomagnetically viable between West Africa, Amazonia, and the paleomagnetically well-constrained Baltica and Laurentia block.

A long-lived connection is usually proposed for Baltica and Laurentia between ~1760 Ma and ~1270 Ma (Salminen et al., 2014). A large distance is observed across the APW path of Baltica between the mean 1265 Ma pole (BA1) (Pesonen et al., 2003), the Salla diabase VGP (BA2) and the 1100–1050 Ma poles (BA3, BA4) (Table 2; Fig. 7A) (Mertanen et al., 1996; Pesonen et al., 2003) and suggests fast drifting at that time. Fast drifting is also observed for Laurentia with the Logan loop and the ~1105–1080 Ma Keweenawan track (LA1-LA2) (Swanson-Hysell et al., 2019). Between ~1050 and 900 Ma the APW

path of Laurentia was defined as the Grenville loop and the same interval in Baltica was defined as the Sveconorwegian loop, but its shape and motion are debated (Elming et al., 2014; Gong et al., 2018). The best attempts to adjust the Grenville and Sveconorwegian loops are along an Euler pole of 75.8°N, 264.2°E, −59.2° (Pisarevsky et al., 2003), or in a tighter fit of 81.5°N, 250°E, −50° (Evans, 2009). However, Baltica rotated ~70° clockwise in relation to Laurentia between the ~1800–1200 Ma NENA (Northern Europe–North America) configuration (Gower et al., 1990) and the ~1050–800 Ma Rodinia configuration (Salminen et al., 2009). These reconstructions imply a single Laurentia–Baltica block between ~1050 and 800 Ma during the Rodinia. Key 951–935 Ma mean poles for Baltica (BA6) confirmed this clockwise motion, but a more complex shape for the APW path is proposed considering the ~971 Ma VGP of Blekinge-Dalarna dykes (Group B) (BA5) (Fig. 7A) (Gong et al., 2018). A late Sveconorwegian group of poles (936–850 Ma) obtained for the Rogaland Igneous Complex (RIC) and the ~860 Ma Hunneden dykes with a stable remanence of same polarity suggest a stable position for Baltica at high latitude (BA7-BA11) (Walderhaug et al., 1999). The primary remanence of this group is supported by an inverse contact test with the ~635 Ma Egersund dyke swarm (Walderhaug et al., 2007).

West Africa is always associated with the Amazonia Craton in the Paleo-Mesoproterozoic reconstructions but in a different position from the Gondwana link (Onstott and Hargraves, 1981). These cratons were juxtaposed with the Baltica in the South America Baltica (SAMBA) connection with the possibility of a long-lived connection between ~1800 and 800 Ma (Johansson, 2009). An alternative reconstruction, using geological considerations, was proposed with Kalahari-Congo, São Francisco and India in the Umkondia supercraton at ~1110 Ma (Choudhary et al., 2019). Using the paleomagnetic poles of the ~1199 Ma Nova Floresta formation (AM1) (D’Agrella-Filho et al., 2008) and ~1149 Ma Fortuna formation (AM2) (Tohver et al., 2002) (Fig. 7A), a strike-slip migration of Amazonia along the Laurentia at ~1200–1150 Ma was initially proposed. But, a preliminary ~1110 Ma paleomagnetic pole for the well-dated Rincón del Tigre Complex (AM3) (Teixeira et al., 2015) supports a moderate to low latitude for Amazonia at that time (Patroni, 2015), which is incompatible with the model of oblique collision proposed by Tohver et al. (2002). These AM3 pole for Amazonia supports the model of Evans (2013) suggesting a clockwise rotation of the Amazonia and Baltica to collide with Laurentia. For West Africa, paleomagnetic results were obtained from the Mesoproterozoic units of the Adrar (NW- West Africa, Mauritania) (Morris and Carmichael, 1978; Perrin et al., 1988; Perrin and Prévot, 1988). Rooney et al. (2010) obtained a new Re—Os age of ~1105 Ma for the Atar group previously estimated at 890–775 Ma. Based on the similarity with younger directions some authors have suggested some remagnetization effects (Perrin and Prévot, 1988; Tohver et al., 2006), but without further evidence the primary origin for their remanence cannot be ruled out. The characteristic component for those rocks is carried by hematite and was revealed at high temperatures (>590 °C). If the magnetization is primary this means the I9 pole (WA1) calculated by Perrin and Prévot (1988) is coeval to the ~1110 Ma Rincón del Tigre pole (AM3) from the Amazonia Craton (Patroni, 2015) (Fig. 7A). No data are available to define the APW path for the Amazonia Craton in Early Neoproterozoic times, but our new ~860 Ma Manso pole satisfies a maximum R-criteria to be considered as an anchor point for paleogeographic reconstructions (Fig. 7A;  $R = 7$ , this study).

The Mesoproterozoic APW path for the Congo-São Francisco Craton is defined by the well-dated Late Kibaran pole (C1) at ~1236 Ma (Meert et al., 1994b). A large shift is observed between the ~1110 Ma pole from the Huile-Epembe dykes (Salminen et al., 2018) and the ~925 Ma poles from the São Francisco dykes (Salvador, Ilhéus, Oliveira) (Fig. 7A) D’Agrella-Filho et al. (1990); (D’Agrella-Filho et al., 2004; Evans et al., 2016). The Congo-São Francisco Craton is usually associated with the Rodinia supercontinent (Merdith et al., 2017), or in a different view connected with the African blocks (D’Agrella-Filho and Cordani, 2017).

**Table 2**

Paleomagnetic database for the Rodinia. Code, Plat – pole latitude, Plon – Pole longitude, Age – nominal age, A95 confidence cones of the paleomagnetic poles used in the paleogeographical reconstructions. R-criteria from Meert et al. (2020). References: Laurentia: [1] Park (1981), [2] Swanson-Hysell et al. (2019), Baltica: [3] Walderhaug et al. (1999), [4] Brown and McEnroe (2004), [5] Stearn and Piper (1984), [6] Walderhaug et al. (2007), [7] Brown and McEnroe (2015), [8] Gong et al. (2018), [9] Mertanen et al. (1996), [10] Pesonen et al. (2003), [11] Salminen et al. (2009), West Africa: [12] This study, [13] Perrin and Prévot (1988), [14] Rooney et al. (2010), Amazonia: [15] Patroni (2015), [16] Teixeira et al. (2015) [17] D'Agrella-Filho et al. (2008), [18] Tohver et al. (2002), Congo-São Francisco: [19] Evans et al. (2016), [20] D'Agrella-Filho et al. (2004), [21] D'Agrella-Filho et al. (1990), [22] Salminen et al. (2018), [23] Meert et al. (1994a), Kalahari: [24] Swanson-Hysell et al. (2015a), North China: [25] Fu et al. (2015), Tarim: [26] Wen et al. (2018).

Code	Name	Age (Ma)	Plat (°N)	Plong (°E)	A <sub>95</sub>	R1	R2	R3	R4	R5	R6	R7	Rc	References
<b>LAURENTIA</b>														
LA3	Basal units from the Little Dal Group	892–849	−15.7	141.3	3.6	0	1	1	1	1	0	0	4	[1]
LA2	1105 Ma synthetic Keweenawan track	1105	42.7	206.4	2.1	–	–	–	–	–	–	–	>5	[2]
LA1	1110 Ma synthetic Keweenawan track	1100	46.3	222.7	3.2	–	–	–	–	–	–	–	>5	[2]
<b>BALTICA</b>														
BA11	Hunnedalen dykes	860	−41	222	10.5	1	1	1	0	1	0	1	5	[3]
BA10	Egersund-Ogna anorthosites	870	−42.1	200.4	9	1	1	1	0	0	0	1	4	[4]
BA9	Other Rogaland anorthosites	870	−43.5	213.7	3.6	1	1	1	0	0	0	1	4	[3, 5]
BA8	Rogaland Igneous Complex (RIC)	870	−45.9	238.4	18.2	1	0	1	1	0	0	1	4	[6]
BA7	Bjerkreim-Sokndal layered intrusion (RIC)	916	−35.9	217.9	6	1	1	1	0	1	0	1	5	[7]
BA6	Mean 951–935 Ma Baltica pole	940	−2.6	239.6	5.8	1	1	1	1	1	1	1	7	[8]
BA5	971 Ma BDD dykes (VGP)	971	−27	230.4	14.9	1	0	1	0	1	1	1	5	[8]
BA4	Laanila-Ristijärvi dykes	1050	−2.1	212.2	16.4	1	0	1	1	1	0	0	4	[9]
BA3	Mean Baltica 1100 Ma	1100	1	208	16	–	–	–	–	–	–	–	–	[10]
BA2	Salla diabase dyke VGP	1122	71	113	8.1	1	0	1	1	1	0	0	4	[11]
BA1	Mean Baltica 1265 Ma	1265	4	158	4	–	–	–	–	–	–	–	–	[10]
<b>WEST AFRICA</b>														
WA2	Manso dykes	860	−28.3	177.6	12.7	1	1	1	1	1	1	1	7	[12] This study
WA1	Atar group, unit I9 (GH-comp)	1105	−41.7	61.2	6.4	1	0	1	0	1	0	0	3	[13, 14]
<b>AMAZONIA</b>														
AM3	Rincón del Tigre Complex	1100	−30	28.5	12.8	1	0	1	0	0	1	1	4	[15, 16]
AM2	Fortuna formation red beds	1149	−59.8	335.9	9	1	1	1	0	1	0	0	4	[17]
AM1	Nova Floresta formation	1199	−24.6	344.6	6.2	1	1	1	0	1	0	0	4	[18]
<b>CONGO-SAO FRANCISCO</b>														
<i>São Francisco</i>														
SF3	Bahia Coastal dykes	924	−7.3	286.4	6.2	1	1	1	1	1	0	1	6	[19]
SF2	Salvador dykes -N	924	−6.4	302.7	15.6	1	1	1	1	1	0	0	5	[20]
SF1	Itajú do Colônia	924	−7.7	291	9.8	1	1	0	1	1	0	0	4	[21]
<i>Congo</i>														
C2	Huila-Epembe dykes	1105	−34.7	256.5	8.7	1	1	1	1	1	1	1	7	[22]
C1	Late Kibaran intrusives	1236	17	292.7	5.9	1	1	1	0	0	0	0	3	[23]
<b>KALAHARI</b>														
K1	Umkomdo grand mean pole	1110	−64	222.1	2.6	1	1	1	1	1	1	1	7	[24]
<b>NORTH CHINA</b>														
NC1	Wangshan sills of Huabei -C	895	52.3	329.3	3.5	1	1	1	1	1	1	0	6	[25]
<b>TARIM</b>														
T1	Salajiazage Group volcanics	880	25.5	217	11.3	1	1	1	1	1	0	0	5	[26]

Similarities in length and shape of the APW paths for Baltica, Amazonia, West Africa, and São Francisco-Congo cratons allow us to build a Master APW path between ~1200 and 850 Ma for these continental units (Fig. 7A). This Master APW path suggests that these blocks were nearby between ~1200 and 850 Ma, forming a single continental entity. This large continental unit, hereafter referred to WABAMGO (West Africa-Baltica-Amazonia-Congo) is represented in Fig. 7B. Geological domains, LIP comparisons, and paleomagnetic data between Baltica, Amazonia, and West Africa support a strong connection between these continents since the Paleoproterozoic using the SAMBA model (Baratoux et al., 2019; D'Agrella-Filho et al., 2016; Terentiev and Santosh, 2020). Our model supports the presence of a long-lived accretionary margin during the Mesoproterozoic times in the western part of Amazonia (Sadowski and Bettencourt, 1996). The orientation of West Africa in relation to Amazonia in the SAMBA model is paleomagnetically viable from ~2100 Ma until ~1400 Ma (D'Agrella-Filho et al., 2016), but a later reorientation is necessary to fit with the classical ~550 Ma Gondwana configuration. In the WABAMGO configuration, the West Africa-Amazonia connection is close to this late Neoproterozoic configuration, suggesting this reorientation could have occurred between ~1400 and

1200 Ma, during the breakup of the Columbia supercontinent. The Sunsás and Sveconorwegian orogens are correlated between Amazonia and Baltica in this model (Fig. 7B). A voluminous Early Tonian mafic magmatism is observed in the São Francisco Craton spanning from ~925 Ma to 850 Ma (Danderfer et al., 2009; Moreira et al., 2020). Similar records of Tonian age magmatism have been reported for the Congo with the Sembé Ouesso (Vicat and Pouplet, 1995), for Baltica with the ~850 Ma Hunnedalen dykes (Walderhaug et al., 1999), for West Africa with the ~860 Manso and ~915 Oda dykes in the south of the craton (Baratoux et al., 2019) and the ~880–850 Iggerda-Taïfast dykes in the Anti-Atlas (Kouyaté et al., 2013). A potential match in Amazonia with these ~870–850 Ma LIPs could be the Makinet dykes (formerly Tampok) that were dated with a K—Ar cooling age of  $809 \pm 58$  Ma (at 2-sigma level) (Delor et al., 2003). Early Tonian rifting is also documented for the northern part of the West African Craton with the volcanoclastic deposits of the ~883 Ma Tachdamt Fm (Bouougri et al., 2020). Coeval Early Tonian extension in West Africa and São Francisco is thus supported by the WABAMGO configuration (Fig. 7B). A rare “Grenvillian event” (~1000–920 Ma) documented within the WABAMGO juxtaposition is the Cariris Velhos tectonic event, proving some continental

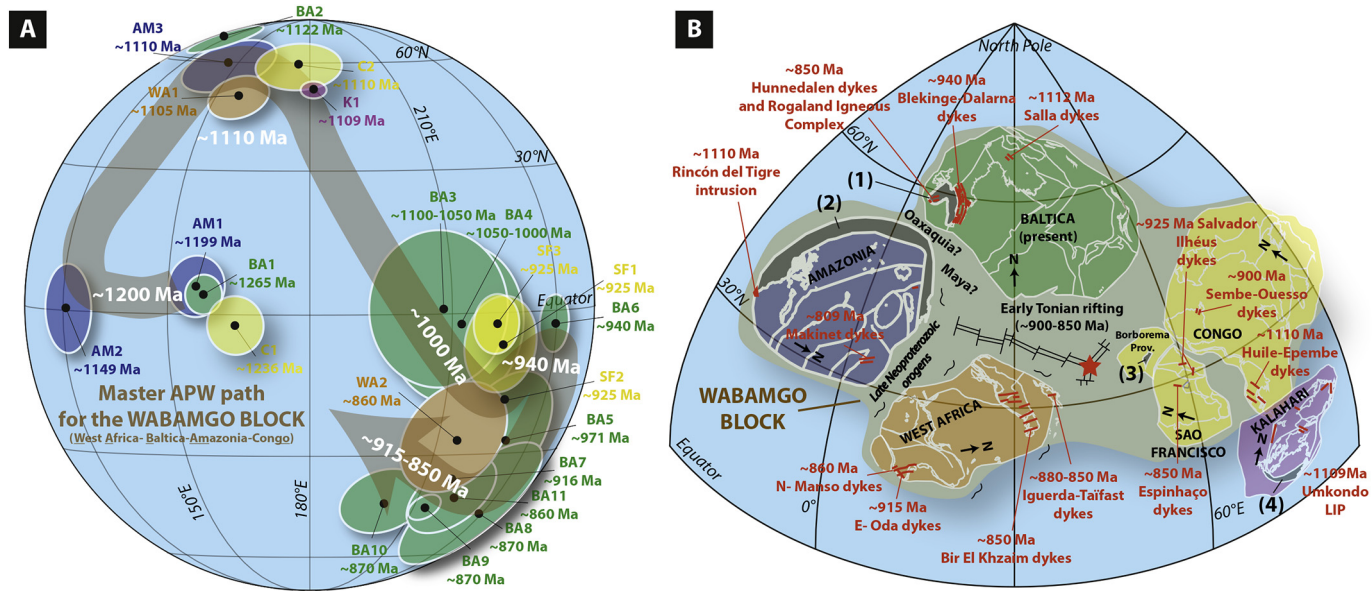


**Fig. 7.** A: The WABAMGO (West Africa-Baltica-Amazonia-Congo) juxtaposition using Baltica as reference frame in present coordinates. Euler poles used in the Baltica reference frame for the different cratons in the WABAMGO configuration: West Africa ( $1.375^{\circ}\text{N}$ ,  $15.1585^{\circ}\text{E}$ ,  $-66.0819^{\circ}$ ), Amazonia ( $10.894^{\circ}\text{N}$ ,  $369.8179^{\circ}\text{E}$ ,  $-89.4471^{\circ}$ ), Congo ( $52.32^{\circ}\text{S}$ ,  $158.71^{\circ}\text{E}$ ,  $-70.57^{\circ}$ ). The São Francisco Craton is rotated to Congo using its pre-Mesozoic configuration ( $46.8^{\circ}\text{N}$ ,  $329.4^{\circ}\text{E}$ ,  $55^{\circ}$ , (McElhinny et al., 2003)). Kalahari is connected to the Congo Craton ( $12.8^{\circ}\text{S}$ ,  $19^{\circ}\text{E}$ ,  $-43.2^{\circ}$ ) according the configuration of Salminen et al. (2018). Present North is indicated for each craton by an arrow. Abbreviations for the  $\sim 1200$ – $1000$  Ma Grenvillian orogens (in black): (1) Sveconorwegian orogen, (2) Sunsás orogen, (3) Cariri Velhos event, (4) Namaqua-Natal orogen. Tonian large igneous provinces (LIPs, in red) are indicated. B: Master apparent polar wander (APW) path for the WABAMGO between  $\sim 1200$  and 850 Ma. Paleomagnetic poles and used abbreviations are listed in the Table 2.

reorganization and convergence at the edge of the mega block of the Borborema Province was followed by a Tonian rifting (dos Santos et al., 2010; Neves et al., 2020).

Detrital zircon ages on Neoproterozoic units from northern and southern West Africa (Ait Lahna et al., 2020; Bouougri et al., 2020; Kalsbeek et al., 2008) indicate “Grenvillian” ages ( $\sim 1250$ – $925$  Ma). The potential sources of these Mesoproterozoic-Neoproterozoic zircon grains could be explained by the proximity of the Grenvillian orogens to the west such as Sunsás and Sveconorwegian and the associated small blocks (e.g. Oaxaquia, Maya), and the Cariri Velhos event to the east. Major shifts in the sedimentation on the West African Craton suggest a complete breakup of the WABAMGO from Baltica and São Francisco-Congo after  $\sim 800$  Ma with the development of subduction zones in northern West Africa in the late Neoproterozoic (Triantafyllou et al., 2016). Following this model, the proximity of the Congo-São Francisco and West Africa may explain the large displacements along the major dextral Transbrasiliano lineament with the closure of the Pharusian Ocean during the assembly of Gondwana in late Neoproterozoic times. The proposed long-lived WABAMGO juxtaposition is geologically and paleomagnetically viable between  $\sim 1200$  and 800 Ma.

### 5.3. Implications for the Rodinia assembly

Using our new Master APW path for the West Africa-Baltica-Amazonia-Congo block, the reconstruction at  $\sim 1110$  Ma shows that the assembly of Rodinia is dominated by the V-shape closure of the external Nuna Ocean (Li et al., 2019), or Grenville Ocean, (Sadowski and Bettencourt, 1996), between the northern Laurentian blocks and the southern WABAMGO (Fig. 8A). This hypothesis of the closure of this Ocean by accretionary orogens was previously suggested on geological grounds (Cawood and Pisarevsky, 2017; Martin et al., 2020), but our study add a paleomagnetic support. The Kalahari Craton is positioned in Fig. 8 along the southern tip of Congo (pos-A) as in (Salminen et al., 2018) or in its inverted position (pos-B) with the Natal-Namaqua orogen

facing the coeval Grenville orogen in Laurentia, in both cases constrained by the  $\sim 1109$  Ma Umkondo pole (K1) (Swanson-Hysell et al., 2015a). In the preferred position B, the Kalahari Craton will collide with the southern coast of Laurentia after the closure of the external Nuna Ocean (Fig. 8B). Nevertheless, the Kalahari position is poorly constrained in Rodinia, and is beyond the scope of this contribution. The orientation of West Africa in the WABAMGO configuration (pos-A, Fig. 8B) differs from the SAMBA model, in which the western margin of West Africa is associated to the southern part of Baltica. Nevertheless, our new proposed configuration requires new Tonian high-quality poles for the unconstrained cratons, especially Amazonia, and new Mesoproterozoic poles for West Africa to confirm the relative orientation between Amazonia and West Africa. Discarding the  $\sim 1105$  Ma WA1 pole, a position closer to the SAMBA model (Johansson, 2009) is paleomagnetically plausible for West Africa (pos-B, Fig. 8B).

For the final paleogeographic configuration at 925–850 Ma we can compare the position of West Africa derived from the Manso paleomagnetic pole with the available record of Laurentia and surrounding blocks (Fig. 8C). Three paleomagnetic poles are available for the northern blocks of Rodinia. Laurentia can be constrained by the basal units from the Little Dal Group, LA3 pole, which passes a fold test, and its age was recently constrained by high-quality correlations between 892 and 849 Ma (Greenman et al., 2020; van Acken et al., 2013). One pole for the Tarim (T1) at  $\sim 880$  Ma (Wen et al., 2018), and one pole for North China at  $\sim 895$  Ma (NC1) (Fu et al., 2015) complete the paleomagnetic database for the northern blocks of Rodinia. Our model implies that Rodinia was formed by extroversion (Murphy and Nance, 2003), with the closure of an external Nuna Ocean between two large blocks, the southern WABAMGO and the northern Laurentian block. Rodinia was finally assembled by a large dextral motion of the Australia-Tarim blocks as suggested by Wen et al. (2018). The polar location of the WABAMGO at  $\sim 900$  Ma, together with the low-mid latitudinal distribution of Laurentia and the blocks of North China, Tarim, Australia (?) confirms a pan-latitudinal rather than an equatorially distributed supercontinent as suggested by Jing et al. (2019).

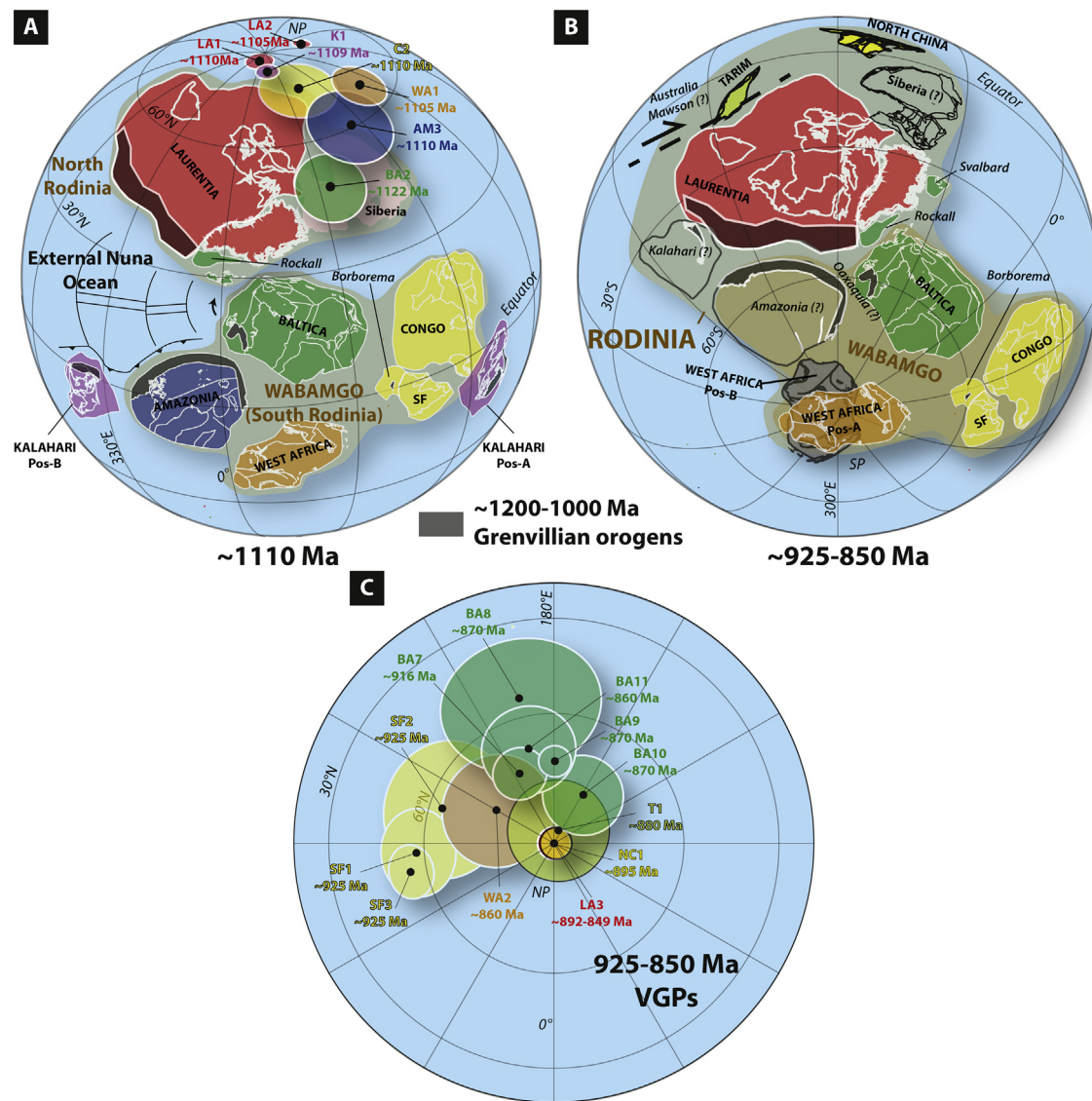


**Fig. 8.** A: Paleogeography reconstruction of the Rodinia assembly at ~1110 Ma showing the presence of the external Nuna Ocean (Grenville Ocean) between the WABAMGO (south Rodinia) and the Laurentia (north Rodinia). Two plausible positions are illustrated for the Kalahari Craton with the Salminen et al. (2018) configuration (pos-A), and Kalahari placed in the west of Amazonia (pos-B) as paleolongitude is arbitrary. We followed the model of Sadowski and Bettencourt (1996) using a subduction toward Amazonia. B: Paleogeography reconstruction of the Rodinia at ~925–850 Ma. Cratons with paleomagnetic constraints (in colors) and cratons with no data (?) are indicated. Two positions of West Africa are illustrated with the position A in agreement with the WABAMGO configuration and the plausible position B according to the uncertainty for the paleolongitude. The hypothesis of a dextral movements from Wen et al. (2018) is indicated for the northern cratons of Australia-Mawson-Tarim. C: Paleomagnetic poles (north pole) used in the reconstruction at ~925–850 Ma (B). See Table 2 for abbreviations and references.

## 6. Conclusions

New U–Pb apatite ages of  $857.2 \pm 8.5$  Ma and  $855 \pm 16$  Ma agree with the previous  $867 \pm 16$  Ma U–Pb baddeleyite age (Baratoux et al., 2019) confirming the extension of the Manso dyke swarm to the north of Ghana. A ~860 Ma Manso key pole ( $28.3^\circ\text{S}$ ,  $177.6^\circ\text{E}$ ,  $A95 = 12.7^\circ$ ,  $R = 7$ ) was calculated and represent the first high-quality paleomagnetic data in Early Tonian for the West African Craton. The remanent magnetization is considered as primary, passing a baked contact test and a reversal test. The paleomagnetic database for West Africa, Baltica, Amazonia, and the Congo-São Francisco cratons supports a long-lived continental unit between ~1200 and 800 Ma, the WABAMGO juxtaposition. During the late Mesoproterozoic-Early Neoproterozoic (~1200–900 Ma), the WABAMGO and the Laurentia were drifting southward. During this migration, a clockwise rotation of the WABAMGO in relation to Laurentia closed the external Nuna

Ocean causing the Grenvillian collisions suturing the Rodinia supercontinent. Thus, this model favors with paleomagnetic support the formation of the Rodinia supercontinent by extroversion.

Supplementary data to this article can be found online at <https://doi.org/10.1016/j.gr.2021.02.010>.

## Sample credit author statement

Paul Yves Jean Antonio: Project administration, Funding acquisition, Conceptualization, Methodology, Investigation, Writing, Original Draft. Lenka Baratoux: Project administration, Supervision, Investigation, Writing. Ricardo I. F. Trindade: Project administration, Supervision, Funding acquisition, Writing. Sonia Rousse: Funding acquisition, Investigation, Writing. Ayite Anani: Investigation, Resources, Writing. Cristiano Lana: Investigation, Validation, Writing. Mélina Macouin: Funding acquisition, Investigation, Writing. Adu Emmanuel W. K.:

Investigation, Writing. Caroline Sanchez: Investigation, Writing. Marco A. L. Silva: Investigation, Validation. Carmen I. Martinez Dopico: Investigation, Writing. Anne-Sophie Firmin: Investigation, Writing. Arnaud Proietti: Resources, Writing. Prince Ofori Ampsonah: Resources, Writing. Patrick Asamoah Sakyi: Resources, Writing.

## Declaration of Competing Interest

The authors declare that they have no known competing financial interests or personal relationships that could have appeared to influence the work reported in this paper.

## Acknowledgements

We would like to thank the editor Joseph G. Meert, Anthony F. Pivarunas and an anonymous reviewer for thoughtful comments and suggestions that allowed us to improve this manuscript. We thank the Brazilian Fundação de Amparo à Pesquisa do Estado de São Paulo (FAPESP grants 2017/18840-6, 2018/23755-0) for financial support of the postdoctoral fellowship (Paul Yves Jean Antonio), and funding of the associated thematic project of Ricardo Ivan Ferreira Trindade (2016/06114-6). We wish to thank the Laboratório de Paleomagnetismo (USPmag) of the University of São Paulo and the associated technicians. We thank the Geological Survey of Authority of Ghana, especially Mahu Eric Nene, for field-trip logistics. We thank the Newmont Company, Ltd. of Ahafo mine and the regional director Paul Morley, for accommodation, accessibility to the site and facilities. We thank Philippe de Parseval and Loic Drigo for help during analytical work in Toulouse, and Pierre Camps for access to his duty standing drill press (Géosciences Montpellier). We thank the infrastructure of “Centro Oceanográfico de Registros Estratigráficos (CORE), Instituto Oceanográfico da Universidade de São Paulo” for using the VSM. Thanks to Helen McFarlane, Stephane Perrouyt and Quentin Masurel for the sampling location preparation. This work would not have been possible without the assistance and hospitality of Ghanaian communities (Amanfro, Domeabra, ...).

## References

- Affaton, P., Rahaman, M.A., Trompette, R., Sougy, J., 1991. The Dahomeyide Orogen: Tectonothermal Evolution and Relationships with the Volta Basin. In: Dallmeyer, R.D., Lécorché, J.P. (Eds.), *The West African Orogens and Circum-Atlantic Correlatives*. Springer, Berlin Heidelberg, Berlin, Heidelberg, pp. 107–122.
- Ait Lahna, A., Youbi, N., Tassinari, C.C.G., Basei, M.A.S., Ernst, R.E., Chaib, L., Barzouk, A., Mata, J., Gártner, A., Admou, H., Boumehdi, M.A., Söderlund, U., Bensalah, M.K., Bodinier, J.-L., Maacha, L., Bekker, A., 2020. Revised stratigraphic framework for the lower Anti-Atlas Supergroup based on U-Pb geochronology of magmatic and detrital zircons (Zenaga and Bou Azzer-El Graara inliers, Anti-Atlas Belt, Morocco). *J. Afr. Earth Sci.* 171, 103946.
- Antonio, P.Y., Baratoux, L., Da Trindade, R.I., Rousse, S., Macouin, M., Firmin, A.-S., Martinez-Dopico, C.I., Anani, A.P.A., Ampsonah, P.O., 2019. Preliminary in phase and out of phase AMS study and paleomagnetism of ~ 870 MA mafic dykes in West Africa (Ghana). In: Letters, L. (Ed.), 2019 Biennial Meeting of Latinmag, Proceedings Rancagua, Chile, pp. 11–17 B18-P.
- Baratoux, L., Söderlund, U., Ernst, R., de Roever, E., Jessell, M., Kamo, S., Naba, S., Perrouyt, S., Metelka, V., Yatte, D., 2019. New U-Pb Baddeleyite Ages of Mafic Dyke Swarms of the West African and Amazonian Cratons: Implication for Their Configuration in Supercontinents Through Time, Dyke Swarms of the World: A Modern Perspective. Springer, pp. 263–314.
- Berndt, T.A., Chang, L., 2019. Waiting for Forcet: accelerating FORC processing 100× using a fast-fourier-transform algorithm. *Geochem. Geophys. Geosyst.* 20, 6223–6233.
- Black, R., Cabo, R., Moussine-Pouchkine, A., Bayer, R., Bertrand, J., Boulle, A., Fabre, J., Lesquer, A., 1979. Evidence for late Precambrian plate tectonics in West Africa. *Nature* 278, 223.
- Bond, G.C., Nickeson, P.A., Komink, M.A., 1984. Breakup of a supercontinent between 625 Ma and 555 Ma: new evidence and implications for continental histories. *Earth Planet. Sci. Lett.* 70, 325–345.
- Bonhomme, M., 1962. Contribution à l'étude Géochronologique de la Plateforme de l'Ouest Africain. *Géologie et Minéralogie*. vol. 5. University of Clermont-Ferrand, Fr Thesis.
- Bouougri, E.H., Lahna, A.A., Tassinari, C.C.G., Basei, M.A.S., Youbi, N., Admou, H., Saquaque, A., Boumehdi, M.A., Maacha, L., 2020. Time constraints on Early Tonian Rifting and Cryogenian Arc terrane-continent convergence along the northern margin of the West African craton: Insights from SHRIMP and LA-ICP-MS zircon geochronology in the Pan-African Anti-Atlas belt (Morocco). *Gondwana Res.* 85, 169–188.
- Brown, L.L., McEnroe, S.A., 2004. Palaeomagnetism of the Egersund-Ogna anorthosite, Rogaland, Norway, and the position of Fennoscandia in the Late Proterozoic. *Geophys. J. Int.* 158, 479–488.
- Brown, L.L., McEnroe, S.A., 2015. 916 Ma Pole for southwestern Baltica: palaeomagnetism of the Bjerkreim-Sokndal layered intrusion, Rogaland Igneous Complex, southern Norway. *Geophys. J. Int.* 203, 567–587.
- Cawood, P.A., Pisarevsky, S.A., 2017. Laurentia-Baltica-Amazonia relations during Rodinia assembly. *Precambrian Res.* 292, 386–397.
- Chew, D.M., Spikings, R.A., 2015. Geochronology and thermochronology using apatite: time and temperature, lower crust to surface. *Elements* 11, 189–194.
- Chew, D.M., Sylvester, P.J., Tubrett, M.N., 2011. U-Pb and Th-Pb dating of apatite by LA-ICPMS. *Chem. Geol.* 280, 200–216.
- Choudhary, B.R., Ernst, R.E., Xu, Y.G., Evans, D., de Kock, M., Meert, J., Ruiz, A., Lima, G.A., 2019. Geochemical characterization of a reconstructed 1110 Ma Large Igneous Province. *Precambrian Res.* 105382.
- Cogné, J.P., 2003. PaleoMac: a MacintoshTM application for treating paleomagnetic data and making plate reconstructions. *Geochem. Geophys. Geosyst.* 4, 1007.
- Condie, K.C., 2002. The supercontinent cycle: are there two patterns of cyclicity? *J. Afr. Earth Sci.* 35, 179–183.
- D'Agrella-Filho, M.S., Cordani, U.G., 2017. The Paleomagnetic Record of the São Francisco-Congo Craton. In: Heilbron, M., Cordani, U.G., Alkmim, F.F. (Eds.), *São Francisco Craton, Eastern Brazil: Tectonic Genealogy of a Miniature Continent*. Springer International Publishing, Cham, pp. 305–320.
- D'Agrella-Filho, M.S., Pacca, I.G., Renne, P.R., Onstott, T.C., Teixeira, W., 1990. Paleomagnetism of Middle Proterozoic (1.01 to 1.08 Ga) mafic dykes in southeastern Bahia State – São Francisco Craton, Brazil. *Earth Planet. Sci. Lett.* 101, 332–348.
- D'Agrella-Filho, M.S., Pacca, I.G., Trindade, R.I.F., Teixeira, W., Raposo, M.I.B., Onstott, T.C., 2004. Paleomagnetism and 40Ar/39Ar ages of mafic dykes from Salvador (Brazil): new constraints on the São Francisco craton APW path between 1080 and 1010 Ma. *Precambrian Res.* 132, 55–77.
- D'Agrella-Filho, M.S., Tolhver, E., Santos, J.O.S., Elming, S.-Å., Trindade, R.I.F., Pacca, I.G., Geraldes, M.C., 2008. Direct dating of paleomagnetic results from Precambrian sediments in the Amazon craton: evidence for Grenvillian emplacement of exotic crust in SE Appalachians of North America. *Earth Planet. Sci. Lett.* 267, 188–199.
- D'Agrella-Filho, M.S., Bispo-Santos, F., Trindade, R.I.F., Antonio, P.Y.J., 2016. Paleomagnetism of the Amazonian Craton and its role in paleocontinents. *Br. J. Geol.* 46, 275–299.
- Dalziel, I.W.D., 1997. Overview: neoproterozoic-Paleozoic geography and tectonics: review, hypothesis, environmental speculation. *Geol. Soc. Am. Bull.* 109, 16–42.
- Danderfer, A., De Waele, B., Pedreira, A.J., Nalini, H.A., 2009. New geochronological constraints on the geological evolution of Espinhaço basin within the São Francisco Craton–Brazil. *Precambrian Res.* 170, 116–128.
- Deenen, M.H.L., Langereis, C.G., van Hinsbergen, D.J.J., Biggin, A.J., 2011. Geomagnetic secular variation and the statistics of palaeomagnetic directions. *Geophys. J. Int.* 186, 509–520.
- Delor, C., Lahondère, D., Egal, E., Lafon, J.M., Cocherie, A., Guerrot, C., Truffert, C., Théveniaut, H., Phillips, P., Avelar, G.V., 2003. *Transamazonian Crustal Growth and Reworking as Revealed by the 1: 500,000-Scale Geological Map of French Guiana*. 2nd ed. (*Géologie de la France*).
- Donnadieu, Y., Godderis, Y., Ramstein, G., Nedelec, A., Meert, J., 2004. A “snowball Earth” climate triggered by continental break-up through changes in runoff. *Nature* 428, 303–306.
- dos Santos, E.J., Schmus, W.R.V., Kozuch, M., Neves, B.B.D.B., 2010. The Cariris Velhos tectonic event in Northeast Brazil. *J. S. Am. Earth Sci.* 29, 61–76.
- Dunlop, D., 1974. Thermal enhancement of magnetic susceptibility. *J. Geophys.* 439–451 IF 32.18.40.
- Dunlop, D.J., 2002. Theory and application of the Day plot (Mrs/Ms versus Hcr/Hc). 1. Theoretical curves and tests using titanomagnetite data. *J. Geophys. Res.* 107 EPM4.1–EPM4.22.
- Elming, S.-Å., Pisarevsky, S.A., Layer, P., Bylund, G., 2014. A palaeomagnetic and 40Ar/39Ar study of mafic dykes in southern Sweden: a new Early Neoproterozoic key-pole for the Baltic Shield and implications for Sveconorwegian and Grenville loops. *Precambrian Res.* 244, 192–206.
- Ernst, R.E., Hamilton, M.A., Söderlund, U., Hanes, J.A., Gladkochub, D.P., Okruglin, A.V., Kolotilina, T., Mekhonoshin, A.S., Bleeker, W., LeCheminant, A.N., Buchan, K.L., Chamberlain, K.R., Didenko, A.N., 2016. Long-lived connection between southern Siberia and northern Laurentia in the Proterozoic. *Nat. Geosci.* 9, 464–469.
- Evans, D.A.D., 2009. The palaeomagnetically viable, long-lived and all-inclusive Rodinia supercontinent reconstruction. *Geol. Soc. Lond. Spec. Publ.* 327, 371–404.
- Evans, D.A.D., 2013. Reconstructing pre-Pangean supercontinents. *Geol. Soc. Am. Bull.* 125, 1735–1751.
- Evans, M.E., Wayman, M.L., 1974. An investigation of the role of ultra-fine titanomagnetite intergrowths in palaeomagnetism. *Geophys. J. Int.* 36, 1–10.
- Evans, D.A.D., Trindade, R.I.F., Catelani, E.L., D'Agrella-Filho, M.S., Heaman, L.M., Oliveira, E.P., Söderlund, U., Ernst, R.E., Smirnov, A.V., Salminen, J.M., 2016. Return to Rodinia? Moderate to high palaeolatitude of the São Francisco/Congo craton at 920 Ma. *Geol. Soc. Lond. Spec. Publ.* 424, 167–190.
- Fernie, N., Glorie, S., Jessell, M., Collins, A., 2018. Thermochronological Insights into Reactivation of a Continental Shear Zone in Response to Equatorial Atlantic Rifting (Northern Ghana).
- Feybesse, J.-L., Billa, M., Guerrot, C., Duguey, E., Lescuyer, J.-L., Milesi, J.-P., Bouchot, V., 2006. The paleoproterozoic Ghanaian province: geodynamic model and ore controls, including regional stress modeling. *Precambrian Res.* 149, 149–196.
- Fisher, R., 1953. Dispersion on a sphere. *Proc. Royal Soc. Lond. Ser. A Math. Phys. Sci.* 217, 295–305.

- Fu, X., Zhang, S., Li, H., Ding, J., Li, H., Yang, T., Wu, H., Yuan, H., Lv, J., 2015. New paleomagnetic results from the Huabei Group and Neoproterozoic mafic sills in the North China Craton and their paleogeographic implications. *Precambrian Res.* 269, 90–106.
- Gong, Z., Evans, D.A.D., Elming, S.-Å., Söderlund, U., Salminen, J.M., 2018. Paleomagnetism, magnetic anisotropy and U-Pb baddeleyite geochronology of the early Neoproterozoic Blekinge-Dalarna dolerite dykes, Sweden. *Precambrian Res.* 317, 14–32.
- Gower, C., Ryan, A., Rivers, T., 1990. Mid-Proterozoic Laurentia-Baltica: an overview of its geological evolution and a summary of the contributions made by this volume. *Mid-Proterozoic Laurentia-Baltica* 38, 1–20.
- Greenman, J.W., Rainbird, R.H., Turner, E.C., 2020. High-resolution correlation between contrasting early Tonian carbonate successions in NW Canada highlights pronounced global carbon isotope variations. *Precambrian Res.* 346, 105816.
- Haggerty, S.E., 1991. Oxide textures; a mini-atlas. *Rev. Mineral. Geochem.* 25, 129–219.
- Hartz, E.H., Torsvik, T., 2002. Baltica upside down: a new plate tectonic model for Rodinia and the Iapetus Ocean. *Geology* 30, 255–258.
- Heaman, L.M., LeCheminant, A.N., 2001. Anomalous U-Pb systematics in mantle-derived baddeleyite xenocrysts from île Bizard: evidence for high temperature radon diffusion? *Chem. Geol.* 172, 77–93.
- Hoffman, P.F., 1991. Did the breakout of Laurentia turn Gondwanaland inside-out? *Science* 252, 1409.
- Jessell, M., Santoul, J., Baratoux, L., Youbi, N., Ernst, R.E., Metelka, V., Miller, J., Perrotout, S., 2015. An updated map of West African Mafic Dykes. *J. Afr. Earth Sci.* 112, 440–450.
- Jing, X., Yang, Z., Evans, D.A.D., Tong, Y., Xu, Y., Wang, H., 2019. A pan-latitudinal Rodinia in the Tonian true polar wander frame. *Earth Planet. Sci. Lett.* 115880.
- Johansson, Å., 2009. Baltica, Amazonia and the SAMBA connection—1000 million years of neighbourhood during the Proterozoic? *Precambrian Res.* 175, 221–234.
- Kalsbeek, F., Frei, D., Affaton, P., 2008. Constraints on provenance, stratigraphic correlation and structural context of the Volta basin, Ghana, from detrital zircon geochronology: an Amazonian connection? *Sediment. Geol.* 212, 86–95.
- Kirschvink, J., 1978. The Precambrian-Cambrian boundary problem: paleomagnetic directions from the Amadeus Basin, Central Australia. *Earth Planet. Sci. Lett.* 40, 91–100.
- Kirschvink, J.L., 1980. The least-squares line and plane and the analysis of palaeomagnetic data. *Geophys. J. Int.* 62, 699–718.
- Kirschvink, J.L., Kopp, R.E., Raub, T.D., Baumgartner, C.T., Holt, J.W., 2008. Rapid, precise, and high-sensitivity acquisition of paleomagnetic and rock-magnetic data: development of a low-noise automatic sample changing system for superconducting rock magnetometers. *Geochem. Geophys. Geosyst.* 9.
- Kouyaté, D., Söderlund, U., Youbi, N., Ernst, R., Hafid, A., Ikenne, M., Soulaimani, A., Bertrand, H., El Janati, M.H., R'Kha Chaham, K., 2013. U-Pb baddeleyite and zircon ages of 2040 Ma, 1650 Ma and 885 Ma on dolerites in the West African Craton (Anti-Atlas inliers): possible links to break-up of Precambrian supercontinents. *Lithos* 174, 71–84.
- Li, Z.X., Li, X.H., Kinny, P.D., Wang, J., Zhang, S., Zhou, H., 2003. Geochronology of Neoproterozoic syn-rift magmatism in the Yangtze Craton, South China and correlations with other continents: evidence for a mantle superplume that broke up Rodinia. *Precambrian Res.* 122, 85–109.
- Li, Z.X., Evans, D.A.D., Zhang, S., 2004. A 90° spin on Rodinia: possible causal links between the Neoproterozoic supercontinent, superplume, true polar wander and low-latitude glaciation. *Earth Planet. Sci. Lett.* 220, 409–421.
- Li, Z.X., Bogdanova, S.V., Collins, A.S., Davidson, A., De Waele, B., Ernst, R.E., Fitzsimons, I.C.W., Fuck, R.A., Gladkochub, D.P., Jacobs, J., Karlstrom, K.E., Lu, S., Natapov, L.M., Pease, V., Pisarevsky, S.A., Thrane, K., Vernikovsky, V., 2008. Assembly, configuration, and break-up history of Rodinia: a synthesis. *Precambrian Res.* 160, 179–210.
- Li, Z.-X., Evans, D.A.D., Halverson, G.P., 2013. Neoproterozoic glaciations in a revised global palaeogeography from the breakup of Rodinia to the assembly of Gondwanaland. *Sediment. Geol.* 294, 219–232.
- Li, Z.X., Mitchell, R.N., Spencer, C.J., Ernst, R., Pisarevsky, S., Kirscher, U., Murphy, J.B., 2019. Decoding Earth's Rhythms: Modulation of Supercontinent Cycles by Longer Superocean Episodes.
- Ludwig, K., 2009. Isoplot 4.1. A geochronological toolkit for Microsoft Excel. Berkeley Geochronology Center Special Publication. 4, p. 76.
- Maloof, A.C., Halverson, G.P., Kirschvink, J.L., Schrag, D.P., Weiss, B.P., Hoffman, P.F., 2006. Combined paleomagnetic, isotopic, and stratigraphic evidence for true polar wander from the Neoproterozoic Akademikerbreen Group, Svalbard, Norway. *Geol. Soc. Am. Bull.* 118, 1099–1124.
- Martin, E.L., Spencer, C.J., Collins, W.J., Thomas, R.J., Macey, P.H., Roberts, N.M.W., 2020. The core of Rodinia formed by the juxtaposition of opposed retreating and advancing accretionary orogens. *Earth Sci. Rev.* 103413.
- McDowell, F.W., McIntosh, W.C., Farley, K.A., 2005. A precise 40Ar–39Ar reference age for the Durango apatite (U-Th)/He and fission-track dating standard. *Chem. Geol.* 214, 249–263.
- McElhinny, M.W., Powell, C.M., Pisarevsky, S.A., 2003. Paleozoic terranes of eastern Australia and the drift history of Gondwana. *Tectonophysics* 362, 41–65.
- McFadden, P.L., McElhinny, M.W., 1990. Classification of the reversal test in palaeomagnetism. *Geophys. J. Int.* 103, 725–729.
- McFadden, P.L., Merrill, R.T., McElhinny, M.W., 1988. Dipole/quadrupole family modeling of paleosecular variation. *J. Geophys. Res. Solid Earth* 93, 11583–11588.
- Meert, J.G., 2001. Growing gondwana and rethinking rodinia: a paleomagnetic perspective. *Gondwana Res.* 4, 279–288.
- Meert, J.G., 2014. Strange attractors, spiritual interlopers and lonely wanderers: the search for pre-Pangean supercontinents. *Geosci. Front.* 5, 155–166.
- Meert, J.G., Torsvik, T.H., 2003. The making and unmaking of a supercontinent: rodinia revisited. *Tectonophysics* 375, 261–288.
- Meert, J.G., Hargraves, R.B., Van der Voo, R., Hall, C.M., Halliday, A.N., 1994a. Paleomagnetic and 40Ar/39Ar studies of Late Kibaran intrusives in Burundi, East Africa: implications for Late Proterozoic supercontinents. *J. Geol.* 102, 621–637.
- Meert, J.G., Hargraves, R.B., Van der Voo, R., Hall, C.M., Halliday, A.N., 1994b. Paleomagnetic and Studies of Late Kibaran Intrusives in Burundi, East Africa: Implications for Late Proterozoic Supercontinents. *J. Geol.* 102, 621–637.
- Meert, J.G., Pivarunas, A.F., Evans, D.A.D., Pisarevsky, S.A., Pesonen, L.J., Li, Z.-X., Elming, S.-Å., Miller, S.R., Zhang, S., Salminen, J.M., 2020. The magnificent seven: a proposal for modest revision of the Van der Voo (1990) quality index. *Tectonophysics* 790, 228549.
- Merdith, A.S., Collins, A.S., Williams, S.E., Pisarevsky, S., Foden, J.F., Archibald, D., Blades, M.L., Alessio, B.L., Armistead, S., Plavsa, D., Clark, C., Müller, R.D., 2017. A full-plate global reconstruction of the Neoproterozoic. *Gondwana Res.* 50, 84–134.
- Mertanen, S., Pesonen, L., Huhma, H., 1996. Palaeomagnetism and Sm-Nd ages of the Neoproterozoic diabase dykes in Laanila and Kautokeino, northern Fennoscandia. *Geol. Soc. Lond., Spec. Publ.* 112, 331–358.
- Moores, E.M., 1991. Southwest U.S.-East Antarctic (SWEAT) connection: a hypothesis. *Geology* 19, 425–428.
- Moreira, H.F., Danderfer, A., Costa, A.F.O., Bersan, S.M., Lana, C.C., Queiroga, G.N., 2020. Record of early Tonian mafic magnetism in the central Espinhaço (Brazil): new insights for break-up of the Neoproterozoic landmass ancestor of São Francisco-Congo paleocontinent. *Geosci. Front.* 11, 2323–2337.
- Morris, W., Carmichael, C., 1978. Paleomagnetism of some late Precambrian and lower Palaeozoic sediments from L'Adrar de Mauritanie, West Africa. *Can. J. Earth Sci.* 15, 253–262.
- Müller, R.D., Cannon, J., Qin, X., Watson, R.J., Gurnis, M., Williams, S., Pfaffelmoser, T., Seton, M., Russell, S.H.J., Zahirovic, S., 2018. GPlates: building a virtual earth through deep time. *Geochem. Geophys. Geosyst.* 19, 2243–2261.
- Murphy, J.B., Nance, R.D., 2003. Do supercontinents introvert or extrovert?: Sm-Nd isotope evidence. *Geology* 31, 873–876.
- Neves, S.P., Teixeira, C.M.L., Bruguier, O., 2020. 870–850 Ma-old magmatic event in eastern Borborema Province, NE Brazil: Another Tonian failed attempt to break up the São Francisco Paleoplate? *J. S. Am. Earth Sci.* 102917.
- Niu, J., Li, Z.-X., Zhu, W., 2016. Palaeomagnetism and geochronology of mid-Neoproterozoic Yanbian dykes, South China: implications for a c. 820–800 Ma true polar wander event and the reconstruction of Rodinia. *Geol. Soc. Lond., Spec. Publ.* 424, 191–211.
- Onstott, T., Hargraves, R.B., 1981. Proterozoic transcurrent tectonics: palaeomagnetic evidence from Venezuela and Africa. *Nature* 289, 131–136.
- Palencia-Ortas, A., Ruiz-Martínez, V.C., Villalain, J.J., Osete, M.L., Vegas, R., Touil, A., Hafid, A., McIntosh, G., van Hinsbergen, D.J.J., Torsvik, T.H., 2011. A new 200 Ma paleomagnetic pole for Africa, and paleo-secular variation scatter from Central Atlantic Magmatic Province (CAMP) intrusives in Morocco (Ighrem and Foum Zguid dykes). *Geophys. J. Int.* 185, 1220–1234.
- Park, J., 1981. Analysis of the multicomponent magnetization of the Little Dal Group, MacKenzie Mountains, Northwest Territories, Canada. *J. Geophys. Res. Solid Earth* 86, 5134–5146.
- Patroni, O.A.L., 2015. Estudo Paleomagnético do Complexo Máfico-ultramáfico Rincón del Tigre-Sudeste da Bolívia, Cráton Amazônico, Instituto de Astronomia, Geofísica e Ciências Atmosféricas. Dissertação de Mestrado. Universidade de São Paulo (USP), p. 119.
- Perrin, M., Prévôt, M., 1988. Uncertainties about the Proterozoic and Paleozoic polar wander path of the West African craton and Gondwana: evidence for successive remagnetization events. *Earth Planet. Sci. Lett.* 88, 337–347.
- Perrin, M., Elston, D.P., Moussine-Pouchkine, A., 1988. Paleomagnetism of Proterozoic and Cambrian Strata, Adrar de Mauritanie, CRatonic West Africa. *J. Geophys. Res. Solid Earth* 93, 2159–2178.
- Pesonen, L.J., Elming, S.-Å., Mertanen, S., Pisarevsky, S., D'Agurella-Filho, M.S., Meert, J.G., Schmidt, P.W., Abrahamsen, N., Bylund, G., 2003. Palaeomagnetic configuration of continents during the Proterozoic. *Tectonophysics* 375, 289–324.
- Piper, J.D.A., 2007. The neoproterozoic supercontinent palaeopangaea. *Gondwana Res.* 12, 202–227.
- Piper, J.D.A., Lomax, K., 1973. Palaeomagnetism of Precambrian Birrimian and Tarkwaian Rocks of West Africa. *Geophys. J. Int.* 34, 435–450.
- Pisarevsky, S.A., Natapov, L.M., 2003. Siberia and Rodinia. *Tectonophysics* 375, 221–245.
- Pisarevsky, S.A., Wingate, M.T.D., Powell, C.M., Johnson, S., Evans, D.A.D., 2003. Models of Rodinia assembly and fragmentation. *Geol. Soc. Lond., Spec. Publ.* 206, 35–55.
- Pisarevsky, S.A., Natapov, L.M., Donskaya, T.V., Gladkochub, D.P., Vernikovsky, V.A., 2008. Proterozoic Siberia: a promontory of rodinia. *Precambrian Res.* 160, 66–76.
- Rainbird, R.H., Stern, R.A., Khudoley, A.K., Kropachev, A.P., Heaman, L.M., Sukhorukov, V.I., 1998. U-Pb geochronology of Riphean sandstone and gabbro from Southeast Siberia and its bearing on the Laurentia–Siberia connection. *Earth Planet. Sci. Lett.* 164, 409–420.
- Robert, B., Besse, J., Blein, O., Greff, M., Baudin, T., Lopes, F., Meslouh, S., Belbadaoui, M., 2017. Constraints on the Ediacaran inertial interchange true polar wander hypothesis: a new paleomagnetic study in Morocco (West African Craton). *Precambrian Res.* 295, 90–116.
- Roberts, A.P., Heslop, D., Zhao, X., Pike, C.R., 2014. Understanding fine magnetic particle systems through use of first-order reversal curve diagrams. *Rev. Geophys.* 52, 557–602.
- Rooney, A.D., Selby, D., Houzay, J.-P., Renne, P.R., 2010. Re-Os geochronology of a Mesoproterozoic sedimentary succession, Taoudeni basin, Mauritania: Implications for basin-wide correlations and Re-Os organic-rich sediments systematics. *Earth Planet. Sci. Lett.* 289, 486–496.

- Sadowski, G.R., Bettencourt, J.S., 1996. Mesoproterozoic tectonic correlations between eastern Laurentia and the western border of the Amazon Craton. *Precambrian Res.* 76, 213–227.
- Salminen, J., Pesonen, L.J., Mertanen, S., Vuollo, J., Airo, M.-L., 2009. Palaeomagnetism of the Salla Diabase Dyke, northeastern Finland, and its implication for the Baltica-Laurentia entity during the Mesoproterozoic. *Geol. Soc. Lond., Spec. Publ.* 323, 199–217.
- Salminen, J., Mertanen, S., Evans, D.A.D., Wang, Z., 2014. Paleomagnetic and geochemical studies of the Mesoproterozoic Satakunta dyke swarms, Finland, with implications for a Northern Europe – North America (NENA) connection within Nuna supercontinent. *Precambrian Res.* 244, 170–191.
- Salminen, J., Hanson, R., Evans, D.A.D., Gong, Z., Larson, T., Walker, O., Gumsley, A., Söderlund, U., Ernst, R., 2018. Direct mesoproterozoic connection of the Congo and Kalahari cratons in proto-Africa: strange attractors across supercontinental cycles. *Geology* 46 (11), 1011–1014.
- Samson, S.D., Inglis, J.D., D'Lemos, R.S., Admou, H., Blichert-Toft, J., Hefferan, K., 2004. Geochronological, geochemical, and Nd-Hf isotopic constraints on the origin of Neoproterozoic plagiogranites in the Tasriwine ophiolite, Anti-Atlas orogen, Morocco. *Precambrian Res.* 135, 133–147.
- Sears, J.W., Price, R.A., 1978. The Siberian connection: a case for precambrian separation of the North American and Siberian cratons. *Geology* 6, 267–270.
- Sears, J.W., Price, R.A., 2000. New look at the Siberian connection: no SWEAT. *Geology* 28, 423–426.
- Stacey, J.S., Kramers, J.D., 1975. Approximation of terrestrial lead isotope evolution by a two-stage model. *Earth Planet. Sci. Lett.* 26, 207–221.
- Stearns, J.E.F., Piper, J.D.A., 1984. Palaeomagnetism of the Sveconorwegian mobile belt of the Fennoscandian Shield. *Precambrian Res.* 23, 201–246.
- Swanson-Hysell, N.L., Maloof, A.C., Kirschvink, J.L., Evans, D.A.D., Halverson, G.P., Hurtgen, M.T., 2012. Constraints on Neoproterozoic paleogeography and Paleozoic orogenesis from paleomagnetic records of the Bitter Springs Formation, Amadeus Basin, Central Australia. *Am. J. Sci.* 312, 817–884.
- Swanson-Hysell, N.L., Kilian, T.M., Hanson, R.E., 2015a. A new grand mean palaeomagnetic pole for the 1.11 Ga Umkondo large igneous province with implications for palaeogeography and the geomagnetic field. *Geophys. J. Int.* 203, 2237–2247.
- Swanson-Hysell, N.L., Maloof, A.C., Condon, D.J., Jenkins, G.R.T., Alene, M., Tremblay, M.M., Tesema, T., Rooney, A.D., Haileab, B., 2015b. Stratigraphy and geochronology of the Tambien Group, Ethiopia: evidence for globally synchronous carbon isotope change in the Neoproterozoic. *Geology* 43, 323–326.
- Swanson-Hysell, N.L., Ramezani, J., Fairchild, L.M., Rose, I.R., 2019. Failed rifting and fast drifting: Midcontinent rift development, Laurentia's rapid motion and the driver of Grenvillian orogenesis. *Bulletin* 131, 913–940.
- Teixeira, W., Hamilton, M.A., Lima, G.A., Ruiz, A.S., Matos, R., Ernst, R.E., 2015. Precise ID-TIMS U-Pb baddeleyite ages (1110–1112 Ma) for the Rincón del Tigre–Huanchaca large igneous province (LIP) of the Amazonian Craton: Implications for the Rodinia supercontinent. *Precambrian Res.* 265, 273–285.
- Terentiev, R.A., Santosh, M., 2020. Baltica (East European Craton) and Atlantica (Amazonian and West African Cratons) in the Proterozoic: the pre-Columbia connection. *Earth Sci. Rev.* 210, 103378.
- Thompson, J., Meffre, S., Maas, R., Kamenetsky, V., Kamenetsky, M., Goemann, K., Ehrig, K., Danyshevsky, L., 2016. Matrix effects in Pb/U measurements during LA-ICP-MS analysis of the mineral apatite. *J. Anal. At. Spectrom.* 31, 1206–1215.
- Thomson, S.N., Gehrels, G.E., Ruiz, J., Buchwaldt, R., 2012. Routine low-damage apatite U-Pb dating using laser ablation–multicollector–ICPMS. *Geochem. Geophys. Geost.* 13.
- Tohver, E., van der Pluijm, B.A., Van der Voo, R., Rizzotto, G., Scandola, J.E., 2002. Paleogeography of the Amazon craton at 1.2 Ga: early Grenvillian collision with the Llano segment of Laurentia. *Earth Planet. Sci. Lett.* 199, 185–200.
- Tohver, E., D'Agrella-Filho, M.S., Trindade, R.I.F., 2006. Paleomagnetic record of Africa and South America for the 1200–500 Ma interval, and evaluation of Rodinia and Gondwana assemblies. *Precambrian Res.* 147, 193–222.
- Triantafyllou, A., Berger, J., Baele, J.-M., Diot, H., Ennih, N., Plissart, G., Monnier, C., Watlet, A., Bruguier, O., Spagna, P., Vandycke, S., 2016. The Tachakoucht-Iriri-Tourtit arc complex (Moroccan Anti-Atlas): neoproterozoic records of polyphased subduction-accretion dynamics during the Pan-African orogeny. *J. Geodyn.* 96, 81–103.
- van Acken, D., Thomson, D., Rainbird, R.H., Creaser, R.A., 2013. Constraining the depositional history of the Neoproterozoic Shaler Supergroup, Amundsen Basin, NW Canada: rhenium-osmium dating of black shales from the Wynniatt and Boot Inlet Formations. *Precambrian Res.* 236, 124–131.
- Vandamme, D., 1994. A new method to determine paleosecular variation. *Phys. Earth Planet. Inter.* 85, 131–142.
- Vicat, J.P., Pouclet, A., 1995. Nature du magmatisme lié à une extension pré-panafricaine; les dolerites des bassins de Comba et de Sembe-Ouesso (Congo). *Bulletin de la Société Géologique de France* 166, 355–364.
- Walderhaug, H.J., Torsvik, T.H., Eide, E.A., Sundvoll, B., Bingen, B., 1999. Geochronology and palaeomagnetism of the Hunnedenalen dykes, SW Norway: implications for the Sveconorwegian apparent polar wander loop. *Earth Planet. Sci. Lett.* 169, 71–83.
- Walderhaug, H.J., Torsvik, T.H., Halvorsen, E., 2007. The Eggersund dykes (SW Norway): a robust early Ediacaran (Vendian) palaeomagnetic pole from Baltica. *Geophys. J. Int.* 168, 935–948.
- Wen, B., Evans, D.A., Wang, C., Li, Y.-X., Jing, X., 2018. A positive test for the Greater Tarim Block at the heart of Rodinia: mega-dextral suturing of supercontinent assembly. *Geology* 46 (8), 687–690.
- Wiedenbeck, M., Alle, P., Corfu, F., Griffin, W., Meier, M., Oberli, F.v., Quadt, A.v., Roddick, J., Spiegel, W., 1995. Three natural zircon standards for U-Th-Pb, Lu-Hf, trace element and REE analyses. *Geostand. Newslett.* 19, 1–23.
- Wingate, M.T.D., Pisarevsky, S.A., Evans, D.A.D., 2002. Rodinia connections between Australia and Laurentia: no SWEAT, no AUSWUS? *Terra Nova* 14, 121–128.
- Zijderveld, J., 1967. AC demagnetization of rocks: analysis of results. *Methods Paleomag.* 3, 254.